Spring 5-15-2020

Computation of Knudsen diffusivity in domains with boundary micro-structure

Luis Alberto Garcia German
Washington University in St. Louis

WASHINGTON UNIVERSITY IN ST. LOUIS

Department of Mathematics

Dissertation Examination Committee:

Renato Feres, Chair

Likai Chen

Todd Kuffner

Ari Stern

Gregory Yablonsky

Computation of Knudsen Diffusivity in Domains With Boundary Micro-structure

by

Luis Garcia German

A dissertation presented to

The Graduate School

of Washington University in

partial fulfillment of the

requirements for the degree

of Doctor of Philosophy

May 2020

St. Louis, Missouri

Table of Contents

Acknowledgments

First and foremost I would like to thank my advisor Renato Feres for his support and mentorship throughout my years in the program. Thanks also to our collaborator Tim Chumley. Their guidance and encouragement are the reason we were able to have a successful research project.

I would also like to extend my gratitude to everyone in the mathematics department. In particular I am grateful to John McCarthy for always being available and willing to help. Also a special thanks to the committee members Likai Chen, Todd Kuffner, Ari Stern, and Gregory Yablonsky for taking the time to evaluate my research.

To all my friends, peers, and teachers - I could not have done this without you. Special thanks to Ruben Arteaga, Paulino Fontes, Stephan Garcia, Guanshengrui Hao, Mohammed Jabbari, Michael Mei, George Nanoski, Alexandru Papiu, Kimberly Parker, Mahmoud Shehadeh, Carlos Urueta, Liquin Yu, Wei Wan, and Tian Wang - their camaraderie and influence are the reason this journey has been fulfilling.

Lastly a very special thank you to mom, my sister Brenda, and my partner Tara for always being there for me.

Luis Garcia German

Washington University, May 2020

Abstract of the Dissertation

Computation of Knudsen Diffusivity in Domains With Boundary Micro-structure

by

Garcia German, Luis

Doctor of Philosophy in Mathematics,

Washington University in St. Louis, 2020.

Professor Renato Feres, Chair

We develop an analytical framework and numerical methods for the determination of the coefficient of self-diffusivity for the transport of a rarefied gas in channels, in the limit of large Knudsen number. We provide an effective method for determining the influence of channel surface micro-structure on the value of diffusivity. We also show how characteristic numbers of the system, namely geometric parameters of the micro-structure, the spectral gap of a Markov transition operator defined for a given micro-structure, and the tangential momentum accommodation coefficient of a commonly used model of surface scattering, are related. Examples of micro-structures are investigated regarding the relation of these quantities numerically and analytically.

1. Introduction

The mathematical problems investigated in this thesis are motivated by the following applied problem. In the idealized experiment shown in Figure 1.1, a pulse of inert gas at low pressure is pumped into a long but finite tube, which we refer to as the *channel.* The inner surface of the channel has some degree of roughness due to its molecular structure and surface irregularities. The experimenter is able to measure the rate of gas outflow using some device such as a mass spectrometer, which generates data of the kind represented by the graph on the right-hand side of the figure. From such data transport characteristics of the gas flow through the channel can be derived, as described in [1]. We assume a sufficiently small pulse, under vacuum conditions, to insure that molecular mean free path is much larger than the diameter of the channel. Thus collisions between the gas molecules can be ignored while gas-surface interaction is expected to influence transport properties most prominently. The property of interest here, which can be indirectly measured from such an experiment, is the Knudsen self-diffusivity coefficient of the gas, as explained, for example, in [1]. The central question we wish to address is: How do the surface characteristics affect the Knudsen self-diffusivity?

In this thesis, we assume that gas-surface interaction amounts to perfectly elastic, or billiard-like, collisions between point masses (the *gas molecules*, also referred to here as *particles*) and the channel surface, hence energy exchange between surface and molecules will be ignored. We assume moreover that the channel is two-dimensional and that its

surface micro-structure is static and periodic, and can be described by a relatively small number of geometric parameters. Thus the mathematical problem we pose here is to determine how the Knudsen self-diffusivity explicitly depends on these parameters. We identify this diffusivity with the variance of a limit Wiener process, as explained later.

The analysis developed in this thesis does not require in an essential way all the assumptions just made. In a future work we will consider three-dimensional cylindrical channels and allow for energy exchange between gas and surface at a given surface temperature. But the greater simplicity of the present set-up will help to make clearer the main points.

In the large Knudsen number limit (i.e., for large mean free paths), molecular trajectories are independent of each other and the diffusion process is derived from an analysis of individual trajectories of particles undergoing a random flight inside the channel. This random flight is governed by a Markov operator P that gives, at each particle-surface collision, the post-collision velocity of the particle as a random function of the pre-collision velocity. All the information about the periodic surface geometry relevant to the task of obtaining diffusivity is encoded in P. In fact, diffusivity corresponds to the variance of a one-dimensional Wiener process obtained from the random flight determined by P via a Central Limit Theorem. (As explained in [1], this variance can be obtained from the mean exit time in the limit of long channel lengths. The mean exit time, as a function of the channel length, is the only information that needs to be extracted from the exit flow rate data. We won't deal here with this particular aspect of the analysis and assume, in effect, that the channel is infinite in length.) Our two main goals are, first, to derive the functional dependence of the variance on the geometric parameters and, second,

obtain effective numerical methods for finding this dependence for any given geometric micro-structure.

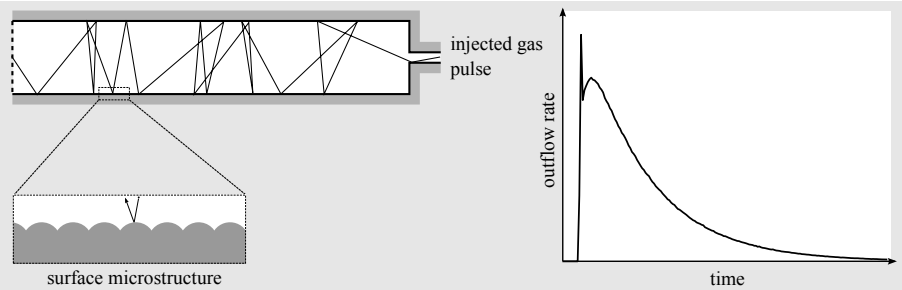

Figure 1.1. Idealized experiment for measuring diffusivity of a rarefied gas flow through a channel. In the limit of large mean free path, trajectories of gas molecules (point masses) injected into the channel as a short pulse, are independent of each other and their stochastic behavior provides information about the geometric micro-structure of the inner surface of the channel. From exit flow rate data one determines the Knudsen self-diffusivity. The mathematical problem posed in this thesis is the explicit determination of the diffusivity constant as a function of geometric parameters defining the micro-structure.

As a bonus, we establish analytic relations among a few important characteristic quantities of the system. Among these we first have the geometric parameters of the micro-structure. For example, in the case of the surface micro-structure consisting of a periodic pattern of circular bumps (depicted in the lower left corner of Figure 1.1) the relevant parameter is $h = K^2/12$, where K is a dimensionless curvature of the bumps to be defined soon. (This simple geometric model will be used at various places later to illustrate the theory.) The quantity h, referred to in this thesis as the *flatness* of the micro-structure, has a general definition that applies to an essentially arbitrary periodic micro-structure, as will be seen. It is closely related to the *tangential momentum accommodation coefficient* ϑ expressing the fraction of collisions that reflect diffusely in the Maxwell-

Smoluchowski collision model. (For a more detailed discussion of ϑ see, for example, [2], where this quantity is denoted f. The flatness parameter was introduced in [3].) A second set of characteristic numbers is the spectrum of P, in particular its *spectral gap*. It has been shown previously that P (see, for example, [4] or [5]; more details will be given in Chapter 3 of the present thesis) is a self-adjoint operator on an appropriate Hilbert space, often compact or quasi-compact, thus having a positive spectral gap. Finally, we have the dimensionless coefficient of self-diffusivity η. This is defined as the quotient of the Knudsen self-diffusivity of the given system over the Knudsen self-diffusivity of the corresponding i.i.d. random flight, for which $\vartheta = 1$. (In this thesis, the term "(Knudsen) self-diffusivity," or simply "diffusivity," common in the applied literature, will simply refer to the variance of the Wiener process obtained as the limit of the random flight in long channels.)

An explicit expression of the diffusivity as an integral over the spectrum of P can be obtained from [6] as will be seen in Chapter 2. Numerical experiments will show, in fact, that often the spectral gap largely determines the diffusivity and thus η. A close connection between the flatness parameter and the spectral gap of P can be derived from a perhaps surprising relationship between P, for general micro-structures with small h, and the Legendre differential operator. The latter arises as the infinitesimal generator of the diffusion in (post-collision) velocity space when the surface exhibits a relatively small degree of roughness (equivalently, small values of h, or small values of the accommodation coefficient ϑ).

The second central concern of this thesis is to obtain and validate effective numerical methods for computing the self-diffusivity in terms of the geometric micro-structure

parameters. This will be discussed in detail in Chapter 4. A number of numerical experiments involving different micro-structures will also be explored.

Better understanding of rarefied gas transport has practical implications for a number of engineering fields including high altitude gas dynamics, porous media, vacuum technology, nano- and microfluidics, among others. These applications have stimulated much experimental work. The following list of papers is a far from thorough or systematic sample of such work: [7–11]. The reader interested in the more applied side of the subject should consult these sources and others cited in them. From a purely mathematical perspective, this is a rich source of well motivated and potentially fruitful problems in the general theory of stochastic processes, and more specifically in the study of the stochastic dynamics of *random billiard systems*. This is our main motivation for studying the subject. We mention from the mathematical literature the following, also necessarily incomplete, list: [12–16].

The rest of this thesis is organized as follows. In Chapter 2 we detail our main results after introducing the necessary definitions. Here we define what we call the *random billiard Markov chain* model in detail and state some of its basic properties. In Chapter 3 we show that under certain geometric conditions on the boundary micro-structure, the Markov chain has positive spectral gap and is uniformly ergodic. Numerical evidence for this is then given for a few examples. With ergodicity in hand, in Chapter 4 we discuss the central limit theory of the Markov chain providing explicit expressions for the variance of the limit diffusion in terms of the Markov operator P. The main analytic technique for computing diffusivity, based on a Galerkin method for solving a Markov-Poisson equation and a key observation that P is closely related to the Legendre differential operator, is also

given in this introductory section. In Chapter 5 this approach for obtaining diffusivity is then compared with other more straightforward methods for a family of micro-structures we call the *simple bumps* family. Chapter 6 described our methodology for obtaining the finite rank approximation of P used for the numerical simulations in this thesis. And we end with a few more numerical examples of micro-structures in Chapter 7, having in mind the relation between geometric parameters, diffusivity, and spectral gap.

2. Main definitions and results

2.1 The billiard cell and its transition operator P

The notation $\mathcal{P}(\Omega)$ will be used below to denote the space of probability measures on a measurable space Ω. If μ is a measure on Ω and $f : \Omega \to \mathbb{R}$ is μ-integrable, we write the integral of f with respect to μ as

$$\mu(f) := \int_\Omega f(\omega)\, \mu(d\omega).$$

The Hilbert space of square integrable functions with respect to μ and its subspace of functions with mean zero will be written

$$L^2(\Omega, \mu) = \left\{ f : \mu\left(f^2\right) < \infty \right\}, \; L^2_0(\Omega, \mu) = \left\{ f \in L^2(\Omega, \mu) : \mu(f) = 0 \right\},$$

with inner product $\langle f, g \rangle_\mu := \int_\Omega f(\omega) g(\omega)\, \mu(d\omega)$ and norm $\|f\|_\mu := \langle f, f \rangle_\mu^{1/2}$. The operator norm will be denoted with $\| \cdot \|_{\text{op}}$.

The general set-up will be that of a two-dimensional *random billiard* with static, periodic, geometric micro-structure, as in [1,3–5,17,18]. The periodic structure is defined by the choice of a *billiard cell* M, from which the Markov operator P will be defined. The billiard cell is a subset M of $\mathbb{T} \times \mathbb{R}$, where $\mathbb{T}$ denotes the 1-dimensional torus (equivalently, the interval $(0, \ell)$ with periodic condition imposed at the endpoints, where ℓ will typically be set equal to 1.) The boundary of the billiard cell is assumed to be a piecewise smooth curve. For some of the results given below, the boundary will be the graph of a piecewise

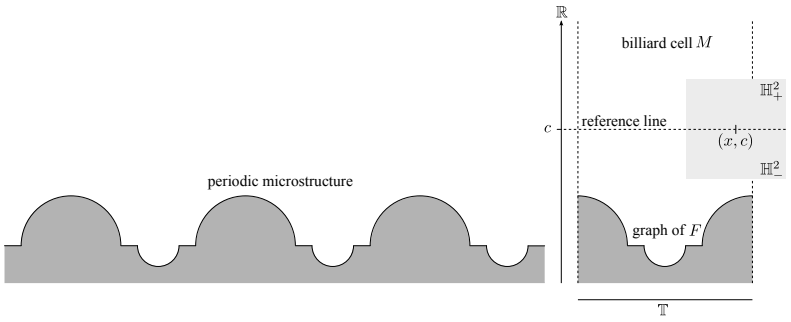

Figure 2.1. A periodic micro-structure and its billiard cell, with some of the notation used to define the random billiard map and its transition operator P. For some of our results we assume that the boundary curve is the graph of a piece-wise smooth function $F : \mathbb{T} \to \mathbb{R}$.

smooth function $F : \mathbb{T} \to \mathbb{R}$, so that M consists of the points (x, y) such that $y \geq F(x)$. Choose an arbitrary value c such that $c > F(x)$ for all $x \in \mathbb{T}$. The line $y = c$ will be called the *reference line*. At any point (x, c) on the reference line we define the half spaces $\mathbb{H}^2_-$ and $\mathbb{H}^2_+$ of incoming and outgoing velocities, respectively. Thus $(x, c, v) \in M \times \mathbb{H}^2_-$ represents the initial conditions of an incoming particle trajectory. These conditions uniquely specify (for almost every x and v) a billiard trajectory: upon hitting a non-corner point on the the cell boundary, the particle reflects specularly without changing speed, and upon crossing a vertical boundary line of M (more precisely, a line separating two adjacent cells, represented in Figure 2.1 by the vertical dashed lines) it reenters the other (dashed) line with unchanged velocity. With probability 1 on the set of initial conditions (due to Poincaré's recurrence), the trajectory returns to the reference line, at which point we register its outgoing velocity $V(x, v) \in \mathbb{H}^2_+$ and new position x'. Without risk of confusion we may identify (though reflection about the reference line) $\mathbb{H}^2_-$ and $\mathbb{H}^2_+$, denoting both by $\mathbb{H}^2$. We have thus defined a transformation $(x, v) \mapsto (x', V(x, v))$ (for

almost all initial conditions (x, v)) on $\mathbb{T} \times \mathbb{H}^2$. We call this transformation the *return billiard map*.

Note that $|v| = |V|$ since collisions are elastic. We may, without loss of generality, assume that the particle trajectories have unit speed. The incoming or outgoing *state space*, consisting of initial or return pairs of position and velocity, can then be taken to be the Cartesian product $(0, \ell) \times \mathcal{X}$, where $\mathcal{X} = (0, \pi)$ is the interval of angles the particle velocity makes with the reference line. We can (and often will) as well define $\mathcal{X} = (-1, 1)$ as the set of values of the cosine of those angles. The phase space itself will be denoted $\mathcal{V} = \mathbb{T} \times \mathcal{X}$.

Let $\mathcal{P}(\mathcal{X})$ denote the space of probability measures on $\mathcal{X}$. Given an incoming velocity v, let us suppose that x is a random variable with the uniform distribution over the interval $(0, \ell)$. Thus $V(x, v)$ becomes a random variable, and we denote its probability measure by ν_v. The map $v \mapsto \nu_v \in \mathcal{P}(\mathcal{X})$ will be called a *scattering event*. We now define the Markov (or transition probabilities) operator P as follows: Let Φ be any bounded and continuous function on $\mathcal{X}$ and define

$$(P\Phi)(v) = E_v[\Phi(V)] = \int_{\mathcal{X}} \Phi(u)\, \nu_v(du).$$

The justification for assuming, at each scattering event, that the point x of entry over the opening of a billiard cell is random and uniformly distributed is due to our regarding the billiard cell as being very small relative to other length scales; any small uncertainty in the incoming velocity will make x nearly fully uncertain. See [18] for a more detailed explanation of this point.

We can also regard P as a map from $\mathcal{P}(\mathcal{X})$ to itself: Given any $\mu \in \mathcal{P}(\mathcal{X})$, let $\mu P \in \mathcal{P}(\mathcal{X})$ be such that for any test function Φ (bounded and continuous),

$$(\mu P)(\Phi) := \mu(P\Phi).$$

Note our convention of representing the integral of a function Φ with respect to a probability measure μ by $\mu(\Phi)$.

The following summarizes the basic properties of P. For their proofs, see [4, 5]. We say that the billiard cell M is *bilaterally symmetric* (or simply *symmetric*) if it is invariant under reflection through the middle vertical line. When the boundary of the cell is the graph of a function F, this means that $F(x) = F(\ell - x)$ for all $x \in (0, \ell)$.

Proposition 2.1.1 *The Markov operator P, for any given billiard cell, has the following properties.*

1. *The measure $\pi \in \mathcal{P}(\mathcal{X})$ given by $\pi(d\theta) = 1/2 \sin\theta \, d\theta$ is stationary of P. That is, $\pi P = \pi$.*

2. *As an operator on $L^2(\mathcal{X}, \pi)$, P has norm 1.*

3. *If M is symmetric, P is self-adjoint and the stationary Markov chain is reversible.*

If the the billiard cell is not bilaterally symmetric, the adjoint of P is still closely related to P as described in [17] and much of the analysis developed in this thesis still applies. For simplicity, we do not consider the more general type of cells here.

2.2 Spectral gap and ergodicity

Let $(X_n)_{n\geq 0}$ be the Markov chain with transition operator P and initial distribution μ. Then the measure μP^n is the law of the nth step X_n. We are interested in the convergence of μP^n to the stationary measure π in the sense of total variation. Recall that the *total variation* of a signed measure μ is defined as

$$\|\mu\|_v := \sup_{A\subset\mathcal{X}} |\mu(A)|.$$

Definition 2.2.1 *A Markov chain with stationary distribution π is* π-a.e. geometrically ergodic *if there exists $0 < \rho < 1$ such that for π-a.e. $x \in \mathcal{X}$ there exists a constant $M_x > 0$ possibly dependent on x such that $\|\delta_x P^n - \pi\|_v \leq M_x \rho^n$, for all $n \geq 1$.*

The operator P has *spectral gap* if there exists a constant $0 < \rho < 1$ such that

$$\|P\Phi\|_\pi \leq \rho \|\Phi\|_\pi$$

for all $\Phi \in L_0^2(\mathcal{X}, \pi)$. The value $\gamma := 1 - \rho$ is called the *spectral gap* of P; for emphasis, we will sometimes also refer to γ as the *positive spectral gap*. It is straightforward to see that for a compact and self-adjoint P, ρ is given by the largest eigenvalue of P restricted to $L_0^2(\mathcal{X}, \pi)$ and $\gamma > 0$. Finally, we note that if P has spectral gap and is self-adjoint, then for any initial distribution μ which is absolutely continuous with respect to π, there exists a constant $M_\mu > 0$ such that

$$\|\mu P^n - \pi\|_v \leq M_\mu \rho^n.$$

See [19]. We will prove geometric ergodicity for a large class of micro-structures satisfying certain geometric conditions.

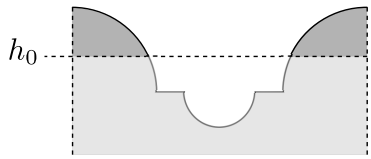

Figure 2.2. An example of billiard cell for which Theorems 2.2.1 and 2.3.1 hold. Other than being bilaterally symmetric, its shape is essentially arbitrary below a line $y = h_0$ whereas above it, the boundary consists of two smooth concave lines with curvature bounded below by some positive number K.

The following is a special case of a more general result to be stated and proved in Chapter 3. We call the *height of the billiard cell* the supremum of the y coordinate function restricted to the boundary of the cell.

Theorem 2.2.1 *Let P be the Markov transition operator for a random billiard Markov chain whose billiard cell is symmetric and satisfies the following property: above a certain $y = h_0$ strictly less than the height of the cell, the cell boundary is the union of smooth, concave curves having curvature bounded away from 0. Then P is a self-adjoint operator with a positive spectral gap. As a result, there exists a constant $\rho \in (0, 1)$ such that for each $\mu \in \mathcal{P}(\mathcal{X})$ with $\|\mu\|_v < \infty$,*

$$\|\mu P^n - \pi\|_v \leq M_\mu \rho^n,$$

for some constant $M_\mu < \infty$ and $n \geq 1$.

Figure 2.2 gives an example of billiard cell for which Theorem 2.2.1 holds.

2.3 Central Limit and Diffusivity

Referring back to Figure 1.1, it is expected for a sufficiently long channel that the molecular random flight can be approximated by a Wiener process whose variance corresponds to the Knudsen self-diffusivity. This is justified by a Central Limit Theorem (CLT). This diffusivity has a convenient expression when the transition operator P is self-adjoint. We describe this expression here and prove further details later in the thesis.

Let $(X_n)_{n\geq 0}$ be, as above, the stationary Markov chain generated by P, with stationary probability measure π. Recall that X_n has values in the space of post-collision velocities $\mathcal{X}$. This space can be parameterized by the values of the cosine of the angle the velocity vector makes with the horizontal reference line $y = c$. (See Figure 2.1.) Thus we may set $\mathcal{X} = (-1, 1)$. Let $f : \mathcal{X} \to \mathbb{R}$ be the observable

$$f(x) = 2rx\left(1 - x^2\right)^{-1/2},$$

where r is the radius of the channel. We suppose, in the context of formulating a CLT for molecular trajectories, that the length of the channel is infinite. Note that $f(X_n)$ is the distance traveled by the particle along the channel's horizontal axis between the n-th and the $n-1$-th collisions with the channel wall. The total horizontal displacement up to the nth collision is

$$S_n(f) = \sum_{k=0}^{n-1} f(X_k).$$

In its standard form, the CLT gives a limit in distribution for expressions of the form $S_n(f)/\sqrt{n}$ where f is an observable having mean zero and finite variance. A simple calculation shows that the horizontal displacement function f has mean zero but infinite

variance. For this reason we consider instead the following modified, cut-off displacement observable:

$$f_a(x) := f(x)\mathbb{1}_{[|f(x)\leq a]}(x) + a\mathbb{1}_{[|f(x)>a]}(x), \tag{2.1}$$

for large $a > 0$. There are a number of physical mechanisms that could be invoked to make this cut-off plausible. For example, the channel might have a slight curvature along its length, setting an upper bound on the horizontal distance traveled. See [2] for an outline of other mechanisms. We should also note that while the CLT with the usual scaling does not hold for the observable f, the distribution of $f(X_n)$ is still in the domain of attraction of the normal law. One can check that f is slowly varying and, as a result, a CLT with nonstandard scaling holds for random billiard Markov chains with sufficient mixing. See [1] for a detailed study of such Markov chains. The program we outline in this thesis to estimate the diffusivity should hold in the infinite variance case as well, but we have chosen to focus on the finite variance case for the sake of clarity of exposition. It should also be noted that for cylindrical channels in dimension 3 (and higher), the observable that gives the distance traveled along the axis of the channel is of finite variance.

We suppose the micro-structure satisfies the same geometric assumptions of Theorem 2.2.1. In particular, P is self-adjoint and has positive spectral gap. Let Π be the *spectral resolution* of P—the projection-valued measure on the spectrum $\sigma(P) \subset [-1, 1]$ granted by the Spectral Theorem for bounded self-adjoint operators. Then

$$P = \int_{-1}^{1} \lambda \, \Pi(d\lambda).$$

Let f be any observable with $\pi(f) = 0$ and $\pi(f^2) < \infty$ (for example, the truncated displacement function f_a) and define the measure Π_f supported on $\sigma(P) \setminus \{1\}$ by

$$\Pi_f(d\lambda) := \langle f, \Pi(d\lambda) f \rangle_\pi.$$

The following is a special case of a theorem that will be stated and proved in Chapter 3.

Theorem 2.3.1 *Let $(X_n)_{n\geq 0}$ be a Markov chain taking values in $\mathcal{X}$ with Markov transition operator P and stationary measure π. Suppose P is associated to a billiard cell satisfying the same geometric assumptions of Theorem 2.2.1. Let $f \in L^2_0(\mathcal{X}, \pi)$. Then $S_n(f)/\sqrt{n}$ converges in distribution to a centered Gaussian random variable $\mathcal{N}(0, \sigma_f^2)$, where the variance is given by*

$$\sigma_f^2 = \int_{-1}^{1} \frac{1+\lambda}{1-\lambda} \Pi_f(d\lambda) = \langle f, f \rangle_\pi + 2\langle f, P(I-P)^{-1} f \rangle_\pi.$$

The expression for the diffusivity given above suggests the following approach for computing σ_f^2. Let $L := P - I$ be the *Markov Laplacian* and g the solution to the *Markov-Poisson equation* $Lg = -f$. Then the dimensionless Knudsen self-diffusivity coefficient takes the form

$$\eta = \frac{\sigma_f^2}{\sigma_0^2} = 1 + 2\|f\|_\pi^{-2} \langle f, Pg \rangle_\pi , \tag{2.2}$$

where $\sigma_0^2 = \|f\|_\pi^2$ is the diffusivity for the process with independent post-collision velocities with the identical distribution π. In the next subsection we explain one approach to carrying out this program by approximating L by an elliptic differential operator $\mathcal{L}$ whose spectral theory is well understood. It turns out that $\mathcal{L}$ has a canonical form as described in the next subsection.

2.4 The Legendre Equation and Diffusion Approximation

Our aim now is to show that it is possible to approximate the solution of the Markov-Poisson equation $Lg = -f$ for a large class of random billiard micro-structures when P is close to the identity operator I. We consider families of micro-structures indexed by a scalar quantity h that, in a sense to be made precise, characterizes a key geometric feature of the microscopic billiard cell, namely its flatness. For each micro-structure with parameter h, the corresponding Markov operator P_h defines the dynamics of the random billiard Markov chain as discussed previously. The key idea now is that for small values h, the operator P_h will act nearly like the identity operator, due to the flatness of the geometry; the Markov-Laplace operator $L_h := P_h - I$, in the limit as $h \to 0$ and under some general assumptions on the microscopic billiard cell, will then have a canonical approximation by the classical Legendre differential operator, whose spectral theory is well understood. In the rest of the subsection, we make explicit the necessary assumptions on the geometry and give the statement of our operator approximation result and provide examples.

Let the boundary of the billiard cell be the graph of a periodic function $F : \mathbb{T} \to \mathbb{R}$. (See Figure 2.1.) Recall that in a scattering event, we have a particle with initial unit velocity $v = (\bar{v}, v_0) \in \mathbb{H}^2$ where $\bar{v}$ is the horizontal (that is, tangent to $\mathbb{T}$) component of v and v_0 the vertical component. The particle enters the billiard cell at a random position $r = (\bar{r}, c) \in \mathbb{T} \times \mathbb{R}$ along the reference line $y = c$. From here, it undergoes geodesic motion until reaching the boundary surface at a point $(x, F(x))$ and reflecting off of it specularly.

After possibly a few further collisions inside the cell, the particle returns to the reference line and exits the cell with a return velocity denoted by $V = (\bar{V}, V_0) \in \mathbb{H}^2$.

In order to characterize how flat the micro-structure boundary is, we consider the normal vector field $n : \mathbb{T} \to \mathbb{R}^2$ along the graph of F, and let $\bar{n}$ denote its projection onto its first component. Finally, we let

$$h := \int_{\mathbb{T}} \bar{n}^2 \, dx = \int_0^1 \frac{F'(x)^2}{1 + F'(x)^2} \, dx. \tag{2.3}$$

It will be seen in examples that h captures information about the curvature of the boundary. For small values of h, the collision events with the boundary will be relatively simple, often resulting in only a single collision with the cell's boundary and only a small deviation from specular reflection. This implies little change in the tangential momentum of the particle with high probability. It is in this sense that h can be thought to have a role similar to the accommodation coefficient ϑ referred to earlier in the thesis.

Let $\mathcal{L}$ denote the differential operator acting on smooth functions $\phi : (-1, 1) \to \mathbb{R}$ as

$$\mathcal{L}\phi(\bar{v}) = \frac{d}{d\bar{v}} \left(\left(1 - \bar{v}^2\right) \frac{d}{d\bar{v}} \phi(\bar{v}) \right). \tag{2.4}$$

Theorem 2.4.1 *Let $(F_h)_{h>0}$ be a family of piece-wise smooth functions $F_h : \mathbb{T} \to \mathbb{R}$ defining bilaterally symmetric billiard cells, indexed by the flatness parameter h introduced in Equation 2.3. Let $(P_h)_{h>0}$ be the corresponding Markov transition operators. Then for any $\phi \in C^3(\mathcal{X})$,*

$$L_h\phi(\bar{v}) = 2h\mathcal{L}\phi(\bar{v}) + O\left(h^{3/2}\right),$$

holds for each v such that every initial condition with velocity v results in a trajectory that collides only once with the boundary of the cell.

In the context of Theorem 2.4.1 we observe that, for each v, every initial condition with velocity v results in a trajectory that collides only once cell boundary if we take h sufficiently small.

The differential operator $\mathcal{L}$ has a well understood spectral theory that will be used to obtain information about P_h. We recall that the eigenvalue problem $\mathcal{L}\phi = \lambda\phi$ has square integrable solutions if and only if λ is of the form $\lambda = -l(l+1)$ for integers $l \geq 0$. The associated eigenfunctions are the Legendre polynomials ϕ_l, $l \geq 0$

$$\phi_0 = 1, \quad \phi_1(x) = x, \quad \phi_2(x) = (3x^2 - 1)/2, \ldots.$$

The collection $(\phi_l)_{l\geq 0}$ forms a complete orthogonal basis for $L^2(-1, 1)$ and

$$\langle \phi_n, \phi_m \rangle := \int_{-1}^{1} \phi_n(x)\phi_m(x)\, dx = \frac{2}{2n+1}\delta_{n,m},$$

where $\delta_{n,m}$ is the Kronecker delta symbol.

As a first application of the approximation given in Theorem 2.4.1, we give an informal estimation of the spectral gap γ_h of P_h for values of h near 0. Note that the largest eigenvalue of P_h is 1, with eigenfunctions given by the constant functions. So γ_h is given by $1 - \lambda$ where λ is the second largest eigenvalue of P_h. Using the approximation in Theorem 2.4.1,

$$P_h\phi_l = (1 - 2hl(l+1))\,\phi_l + O(h^{3/2}),$$

where ϕ_l is the Legendre polynomial associated to eigenvalue $-l(l+1)$. This suggests that the second largest eigenvalue λ of P_h is given by $\lambda \approx 1 - 4h$. Equivalently, this suggests the following asymptotic estimate of γ_h:

$$\gamma_h \approx 4h. \tag{2.5}$$

The idea then will be to use the approximation $\mathcal{L}$ of the Markov-Laplacian L in order to give an approximation of the function $g = (I - P)^{-1} f$ that appears in the equation

$$\sigma_f^2 = \langle f, f \rangle_\pi + 2\langle f, P(I-P)^{-1} f \rangle_\pi ,$$

obtained in Theorem 2.3.1. Note that g is a solution of the Markov-Poisson equation $Lg = -f$. The following thorem shows that a series solution of the Poisson equation for $\mathcal{L}$ can be given explicitly in terms of Legendre polynomials.

Theorem 2.4.2 *Let $(P_h)_{h>0}$ be a family of random billiard Markov transition operators for a family of billiard cells satisfying the geometric assumptions of Theorems 2.3.1 and 2.4.1. For any function $f \in L_0^2(\mathcal{X}, \pi)$, let $\sigma_{f,h}^2$ denote the diffusivity corresponding to P_h. Then*

$$\sigma_{f,h}^2 = -\langle f, f \rangle_\pi + \frac{1}{h} \sum_{l=1}^{\infty} \frac{2l+1}{l(l+1)} \langle \phi_l, f \rangle_\pi^2 + O(h^{1/2}). \tag{2.6}$$

Thus the dimensionless self-diffusivity coefficient can be written as

$$\eta_f = -1 + \frac{1}{h} \sum_{l=1}^{\infty} \frac{2l+1}{l(l+1)} \langle \phi_l, f/\|f\|_\pi \rangle_\pi^2 + O(h^{1/2}) = -1 + \frac{1}{h} C_f + O\left(h^{1/2}\right),$$

where C_f is defined by this identity. Thus, for small h,

$$\eta_f \approx \frac{C_f - h}{h}. \tag{2.7}$$

Then the approximate identity in Equation 2.5 suggests

$$\eta_f \approx \frac{4C_f - \gamma}{\gamma}. \tag{2.8}$$

It is interesting to compare this expression with the one obtained under the Maxwell-Smoluchowski model:

$$\eta = \frac{2 - \vartheta}{\vartheta},$$

where ϑ is the accommodation coefficient, defined as the fraction of diffuse collisions. We thus obtain a conceptual relation linking the purely geometric quantity h (flatness), the spectral quantity γ (spectral gap), and the tangential momentum accommodation coefficient ϑ defined for a standard and widely used collision model. We will explore these approximations numerically for a few examples.

2.4.1 The small bumps micro-structure

Consider the microscopic billiard cell, which we will refer to as the *small bumps* micro-structure throughout the discussion, whose boundary is given by arcs of circles as in Figure 2.3. The geometric parameter of interest here is the dimensionless curvature given by $K = \ell/R$, where R is the radius of one of the arcs and ℓ is the length of the opening to the billiard cell as shown in the figure. An elementary computation using Equation 2.3 gives

$$h = \frac{K^2}{12}.$$

As a result, the spectral gap, approximated for values of K near zero, is given by

$$1 - \lambda \approx 4h = K^2/3.$$

Figure 2.4 shows the numerically obtained values for the spectral gap and η compared to the respective approximations as functions of the dimensionless curvature parameter K.

2.4.2 Summary of the numerical techniques and examples

We describe in this subsection the main numerical method we use for computing the dimensionless self-diffusivity $\eta = \eta_f$ (or, equivalently, the variance σ^2 of the Wiener pro-

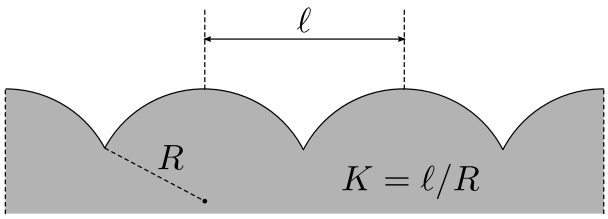

Figure 2.3. The *bumps* micro-structure with dimensionless curvature parameter K.

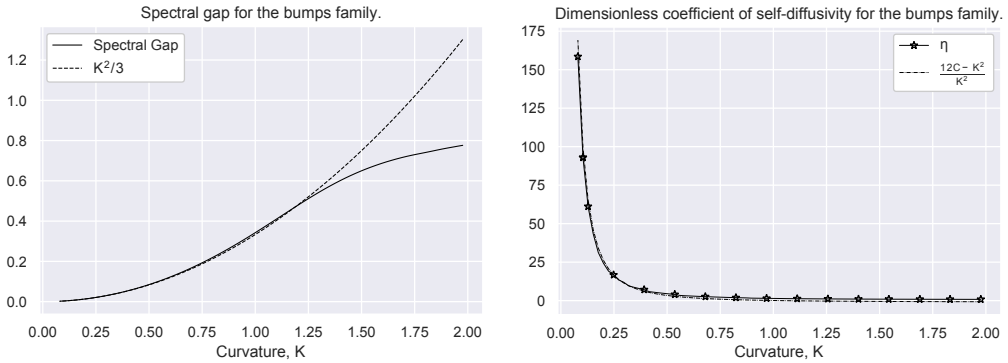

Figure 2.4. Left: the spectral gap of the operator P for the bumps family of micro-structures depicted in Figure 2.3, with dimensionless curvature parameter K, compared with the approximation of the Markov-Laplacian by the Legendre differential operator. The solid curve is constructed from the numerical approximation detailed in Chapter 6. Right: comparison of the dimensionless diffusivity coefficient η obtained using Equation 2.2 and a finite dimensional approximation of P (indicated on the graph by the stars) and the approximation of η as a function of the geometric parameter given by Equation 2.7. The observable is f_a with cut-off $a = 50000$.

cess limit of the random flight in a channel), based on the analytical results summarized in the previous subsection. The observable f is taken here to be the displacement function, denoted f_a earlier, with cut-off $a = 50000$. We also give a few examples of parametric families of geometric micro-structures, emphasizing the dependence of the diffusivity and spectral gap on the parameters.

The starting point is the equation $\sigma^2 = \langle f, f\rangle_\pi + 2\langle f, P(I-P)^{-1}f\rangle_\pi$, which requires that we obtain the solution g to the Markov-Poisson equation

$$(P - I)g = f.$$

This equation can be solved by the Galerkin method in which P is approximated by a finite matrix using the Legendre polynomials as basis elements of $L^2(\mathcal{X}, \pi)$. That this basis is natural for the problem is clearly suggested by Theorem 2.4.2. Thus let $T_n : L^2(\mathcal{X}, \pi) \to R_n$ denote the orthogonal projection to the linear span $R_n = \{\phi_1, \ldots, \phi_n\}$. We define the approximation $g_n \in L^2(\mathcal{X}, \pi)$ of g that solves the finite dimensional linear system $(I - T_nP)g_n = T_nf$; equivalently, we find $g_n \in R_n$ so that

$$\langle (I - P)g_n, \psi\rangle_\pi = \langle f, \psi\rangle,$$

for all $\psi \in R_n$. Writing $g_n = \sum_{j=1}^n \alpha_j\phi_j$ and defining

$$x = (\alpha_1, \ldots, \alpha_n)^T, \quad y = (\langle f, \phi_1\rangle_\pi, \ldots, \langle f, \phi_n\rangle_\pi)^T, \quad G = (\langle \phi_j, \phi_i\rangle_\pi - \langle P\phi_j, \phi_i\rangle_\pi)_{i,j=1}^n,$$

we look for the solution x to $Gx = y$. This gives the solution $g_{\mathrm{GM},n}$ to the finite dimensional linear system, and from it the approximate value $\sigma^2_{\mathrm{GM},,n}$. The following theorem provides an error estimate for this approximation.

Theorem 2.4.3 *Let $f \in L^2_0(\mathcal{X}, \pi)$, where $\mathcal{X} = (-1, 1)$, be such that the first derivative f' is absolutely continuous and the second derivative f'' is of bounded variation. Let σ_f^2 be defined by the equation*

$$\langle f, f\rangle_\pi + 2\left\langle Pf, (I - P)^{-1}f\right\rangle_\pi.$$

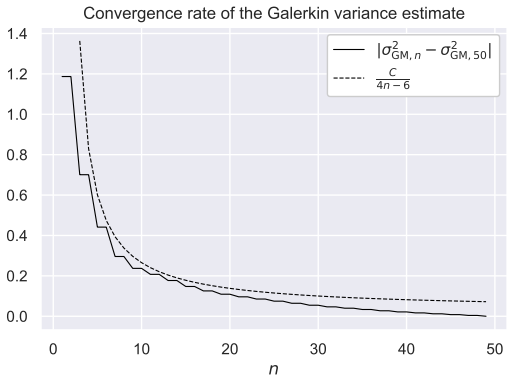

Figure 2.5. Performance of the error bound for the Galerkin approximation of σ_f^2 given in Theorem 2.4.3. Notice the "stair-step" pattern of the graph; the cause for this effect is discussed in Section 5.4.

Then

$$\lim_{n\to\infty} \sigma^2_{\mathrm{GM},n} = \sigma_f^2.$$

Moreover, we have the following rate of convergence:

$$\left|\sigma_f^2 - \sigma^2_{\mathrm{GM},n}\right| \leq \frac{C}{4n-6},$$

where C is a constant depending on f and P but independent of n.

Figure 2.5 illustrates convergence and error bound for $\sigma^2_{\mathrm{GM},n}$ as given by Theorem 2.4.3.

We compare the Galerkin method approach with the other natural ways of obtaining σ_f^2 numerically that are summarized in the following list.

1. Using Equation 2.4.2, we may compute the variance by summing the series involving the Legendre polynomials. (In the graphs of Figure 2.6 we use 500 terms.) The resulting variance will be written $\sigma^2_{\mathrm{Lser},n}$. This is expected to be a good approximation for σ_f^2 when the flatness parameter is small.

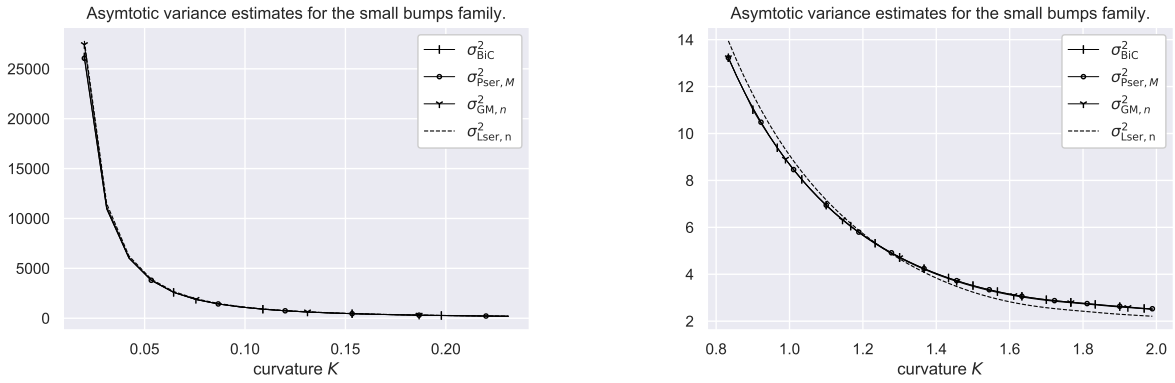

Figure 2.6. Comparing the variance estimates derived from the four approximate solutions of the Markov-Poisson equation for the small bumps micro-structure. On the left (right) is the behavior for small (large) K values. Here we are taking $\sigma^2_{\text{GM},n}$ and $\sigma^2_{\text{Lser},n}$ with $n = 500$; and $\sigma^2_{\text{Pser},M}$ with $M = 10^4$. The markers are there for visual effect and do not represent data points.

2. Using the identity $\sigma^2 = \langle f, f\rangle_\pi + 2\langle f, P(I-P)^{-1}f\rangle_\pi$, we solve the Markov-Poisson equation $(P - I)g = -f$ using a more straightforward finite dimensional approximation of P, as follows. The range of values of the angle that the incoming and outgoing velocities make with the horizontal reference line (see Figure 2.1) is subdivided into 500 equal lengths intervals; then for each such interval we sample the range of initial positions in $(0, 1)$ in equal steps of length 0.0001. The row of P corresponding to angle interval I_i, represented by angle θ_i, is obtained by computing the distribution of outgoing angles of trajectories with initial condition (x, θ_i), where x ranges over the uniformly sampled positions. The linear system is then solved, from which an approximate value of the variance is obtained. We denote this approximate variance σ^2_{BiC}. (The linear system is solved using the bi-conjugate gradient stabilized method, BiCG-stab, thus the notation.)

3. Using the expansion of $(I - P)^{-1}$ into a geometric sum (truncated to 500 terms) and the same matrix approximation of P described above in item 2, we compute the approximate variance, denoted $\sigma^2_{\mathrm{Pser},M}$.

These more straightforward methods are compared with the Galerkin method (for dimension $n = 200$), for the simple bumps family, in the plots of Figure 2.6.

3. Spectral gap and ergodicity

3.1 Decomposing the operator P

We begin this section by introducing a useful technique for decomposing the operator P. The idea will be to condition on the event that a billiard trajectory within the microscopic cell satisfies certain properties, which will allow us to focus attention on geometric features of the micro-geometry that create mixing in the dynamics. More specifically, we show here that under assumptions to be stated, the transition probability operator P for the random billiard Markov chain has a spectral gap by showing that for certain components of the decomposition it is a Hilbert-Schmidt operator. This, along with an additional geometric assumption that yields a reversible Markov chain, in turn will give ergodicity.

Let $N := \{(r, v) \in M \times \mathcal{X} : r = (x, c) \in \mathbb{T} \times \mathbb{R}\}$ be the space of initial conditions of a scattering event and let $N_1, N_2, \ldots$ be a measurable partition of N. Let $N_j(v) := \{x \in \mathbb{T} : (x, c, v) \in N_j\}$. Define $\alpha_j(v) := \lambda(N_j(v))$ for each j and $v \in \mathcal{X}$, where $\lambda \in \mathcal{P}(\mathbb{T})$ is the normalized Lebesgue measure. For each $\Phi \in L^2(\mathcal{X}, \pi)$, define

$$P_j\Phi(v) = \begin{cases} \frac{1}{\alpha_j(v)} \int_{N_j(v)} \Phi(V(r, v))\, dr, & \text{if } \alpha_j(v) \neq 0, \\ 0, & \text{if } \alpha_j(v) = 0. \end{cases} \tag{3.1}$$

The operator P_j will be referred to as the *conditional operator* associated to N_j. Note that $P_j \mathbb{1}_A(v)$ is the conditional probability that the outgoing velocity vector is in $A \subset \mathcal{X}$ given that the pre-collision velocity vector is v and the event N_j holds. Let π_j denote the measure on $\mathcal{X}$ such that $\pi_j(dv) = \alpha_j(v)/(\lambda \otimes \pi)(N_j)\, dv$. Then π_j is the conditional measure given by π conditioned on the event that N_j holds. Finally, observe that for any $\Phi \in L^2(\mathcal{X}, \pi)$, it makes sense to decompose P as follows:

$$P\Phi = \sum_j \alpha_j P_j \Phi. \tag{3.2}$$

We now outline some properties of the conditional operators and the resulting decomposition of P. For details of proofs, see [5].

Proposition 3.1.1 *Let P_j be the conditional operators associated to the measurable partition $N_1, N_2, \ldots$ of the space N of initial conditions of billiard trajectories within billiard microcell M, and let π_j be the conditional measures associated to the partition. Then*

1. *P_j has norm 1.*
2. *Each term $\alpha_j P_j$ in the decomposition has norm at most $\|\alpha_j\|_\infty$.*
3. *If N_j is symmetric—that is, it is invariant under the map $(x, c, v) \mapsto (1 - x, c, Jv)$ where J denotes the reflection across the vertical axis in $\mathbb{H}^2$ and $\mathbb{T}$ is identified with the unit interval— then P_j is self-adjoint as an operator on $L^2(\mathcal{X}, \pi_j)$.*

The following assumptions will be shown to be sufficient for ergodicity.

Assumption 3.1.1 *The microscopic billiard cell is symmetric with respect to reflection across the vertical axis given by the map $(x, y) \mapsto (-x, y)$.*

Assumption 3.1.2 *There exists a measurable partition $N_1, N_2, \ldots$ whose elements are symmetric and such that the following holds for at least one partition element N_j.*

1. *The trajectories with initial conditions in N_j collide only with portions of the boundary of the microscopic billiard cell consisting piecewise smooth concave curves whose curvatures are bounded below by a constant $K > 0$.*

2. $\inf_{v \in \mathcal{X}} \alpha_j(v) > 0$.

Note that these assumptions are not optimal—for example, billiard cells with convex sides have been shown to give geometrically ergodic random billiard Markov chains in [1]—but capture a large class of examples like those in Chapter 2. The key idea of Assumption 3.1.2 is that partitioning the phase space and subsequently decomposing the Markov transition operator into corresponding conditional operators allows us to focus our study of the operator only on the features that create enough dispersion to yield ergodicity.

3.2 Spectral gap for a class of random billiards

Theorem 3.2.1 *Let P be the Markov transition operator for a random billiard Markov chain whose microscopic billiard cell satisfies Assumptions 3.1.1 and 3.1.2. Then P is a self-adjoint operator with spectral gap. As a result, there exists a constant $\rho \in (0, 1)$ such that for each probability measure $\mu \in \mathcal{P}(\mathcal{X})$ with $\|\mu\|_2 < \infty$, there exists a constant $M_\mu < \infty$ such that $\|\mu P^n - \pi\|_v \leq M_\mu \rho^n$.*

Note that Theorem 3.2.1 generalizes Theorem 2.2.1. Indeed, for billiard cells that satisfy the geometric property in the hypotheses of Theorem 2.2.1, it is clear that for each

v, there exists an open set $W_v^1 \subset \mathbb{T}$ such that for each $x \in W_v^1$, the billiard trajectory with initial condition (x, v) results in one collision with the boundary of the billiard cell before returning to the reference line. Letting $N_1 = \{(x, v) : v \in \mathcal{X}, x \in W_v^1\}$ and $N_2 = N \setminus N_1$, it is clear that Assumptions 3.1.1 and 3.1.2 are satisfied.

The proof of Theorem 3.2.1 requires a series of lemmas, which we now introduce. Note that these lemmas are adapted from a series of lemmas in [4] but the present statements have more relaxed hypotheses on the geometry of the billiard cell and thus are slightly stronger.

Before stating the first lemma, we need to introduce some notation. Consider a measurable partition satisfying the conditions in Assumption 3.1.2, where N_j and P_j are the partition element and corresponding conditional operator that satisfy the restrictions in the assumption. Let $W_v := \mathbb{T} \times \{v\}$; we identify W_v with $\mathbb{T}$ for convenience. Let $W_v^i := \{x \in \mathbb{T} : (x, v) \in N_i\}$ for each partition element N_i. For each $v = (\cos\theta, \sin\theta) \in \mathbb{H}^2$ and $x \in \mathbb{T}$, there exists $V(x, v) = (\cos\Theta, \sin\Theta) \in \mathbb{H}^2$ given by the billiard return map applied to a trajectory with initial condition (x, v). We let $\Psi_\theta(x) := \Theta$ denote the function that gives the angle the trajectory makes with the reference line upon exit from the billiard cell.

Lemma 3.2.1 *Suppose the billiard cell satisfies Assumption 3.1.2, with partition element N_j and conditional operator P_j satisfying the conditions in the assumption. Then for all v, the set W_v^j consists of a countable union of open intervals $W_{v,i} \subset \mathbb{T}$. Moreover, the*

restriction $\Psi_{\theta,j} := \Psi_\theta|_{W_{\theta,j}}$ *is a diffeomorphism from* $W_{v,j}$ *onto its image* $V_{v,j}$*. Finally, we have that* $P_j f(\theta) = \int_{\mathcal{X}} f(\phi)\omega(\theta,\phi)\pi_j(d\phi)$ *where*

$$\omega(\theta,\phi) := \frac{(\lambda\otimes\pi)(N_j)}{\alpha_j(\theta)\alpha_j(\phi)} \sum_j \mathbb{1}_{V_{\theta,j}}(\phi) \left(\frac{1}{2}\left|\Psi'_\theta\left(\Psi_\theta^{-1}(\phi)\right)\right|\sin\phi\right)^{-1}, \tag{3.3}$$

and $\mathbb{1}_{V_{\theta,j}}$ *denotes the indicator function of the set* $V_{\theta,j}$*.*

The proof of Lemma 3.2.1 is in Section A.2. The next intermediary lemma gives an estimate on the kernel in Lemma 3.2.1, which will subsequently be used to prove that the kernel is square integrable. Its proof follows from [4, Lemma 6.5] with only minor modifications.

Lemma 3.2.2 *Consider a billiard cell satisfying Assumption 3.1.2 and let* ω *be the kernel given in Equation 3.3. Then for all* $\theta \in (0,\pi)$ *and* $\phi \in \Psi_\theta(W_\theta^j)$*,* $\omega(\theta,\phi) \leq N/(K\sin\phi\sin\theta)$ *where* N *is the number of points of discontinuity* $x \in \mathbb{T}$ *of* $\Psi'_\theta(x)$*.*

The next intermediary lemma gives an estimate on the kernel in Lemma 3.2.1. Its proof follows from [4, Lemmas 6.5, 6.6, 6.7] with only minor modifications.

Lemma 3.2.3 *Consider a billiard cell satisfying Assumption 3.1.2 and let* ω *be the kernel given in Equation 3.3. Then* $\omega \in L^2(\mathcal{X}\times\mathcal{X}, \pi_j\otimes\pi_j)$*.*

The following lemma is adapted from [20, Theorem 9.9]. It will be used to show that for an operator P which admits a decomposition as in Equation 3.2, it suffices to show that one conditional operator is compact in order to prove that P has spectral gap.

Lemma 3.2.4 *Let* K *and* T *be bounded self-adjoint operators on a Hilbert space and suppose that* K *is compact. Then the essential spectrum of* $T+K$ *is contained in the*

essential spectrum of T. In particular, if $\|T+K\|=1$ and $\|T\|<1$, then the spectral gap of $T+K$ satisfies $\gamma(T+K)\geq \min\{1-\|T\|,\gamma(K)\}$.

We conclude with the proof of the section's main theorem.

Proof [Proof of Theorem 3.2.1] That P is self adjoint follows from Assumption 3.1.1 and Proposition 2.1.1. To see that P has spectral gap, we apply Lemma 3.2.4. Using the notation of the lemma, we let $K=\alpha_j P_j$ and $T=\sum_{i\neq j}\alpha_i P_i$. Then, applying Lemmas 3.2.1 and 3.2.3, we have that K is a Hilbert-Schmidt integral operator and hence it is compact. It is clear that T is bounded and self-adjoint and $||T+K||=||P||=1$. Moreover, $1-||T||\geq \inf_{v\in\mathcal{X}}\alpha_j(v)>0$. It follows that the spectral gap of P is strictly positive. The concluding statement of exponential convergence to the stationary measure in total variation then follows immediately using the Cauchy-Schwarz inequality since $||\mu||_v=1/2||\mu||_{L^1}\leq 1/2||\mu||_{L^2}$.

■

4. Diffusivity

4.1 A central limit theorem for Markov chains

Let $f : \mathcal{X} \to \mathbb{R}$ be a function on the state space of the random billiard Markov chain $(X_n)_{n\geq 0}$ with Markov transition operator P. We refer to f as an *observable* (or *functional*) of the Markov chain. Without loss of generality, we suppose that it has mean zero with respect to the stationary distribution: $\pi(f) = 0$. Our focus in this section will be on the limiting distribution (after appropriate scaling) of partial sums of the functional of the Markov chain given by

$$S_n(f) := \sum_{k=0}^{n-1} f(X_k).$$

It is well known that under appropriate mixing conditions for the Markov chain, $S_n(f)/\sqrt{n}$ converges in distribution to a centered Gaussian distribution with variance parameter σ_f^2. As a preliminary result, we show that random billiard Markov chains with micro-structure have sufficiently fast mixing for a (central) limit theorem of this kind to hold. However, our primary focus will be to show that the variance σ_f^2 of the limiting Gaussian distribution, which we refer to as the *diffusivity* of the system, can be rigorously approximated, and formulas can be derived in terms of geometric parameters for families of random billiard micro-structures.

We use here a result adapted from [6], which states that the central limit theorem holds for reversible Markov chains satisfying a non-degeneracy condition on σ_f^2.

Theorem 4.1.1 *Let $(X_n)_{n\geq 0}$ be a Markov chain with stationary measure π and let $f : \mathcal{X} \to \mathbb{R}$ be a function such that $\pi(f) = 0$ and $\pi(f^2) < \infty$. If the Markov chain is reversible, then $S_n(f)/\sqrt{n}$ converges in distrubtion to a centered Gaussian random variable $\mathcal{N}(0, \sigma_f^2)$ as long as $\sigma_f^2 < \infty$.*

In the discussion that follows, it will be useful to express σ_f^2 in terms of the spectrum of P, viewed as an operator on $L^2(\mathcal{X}, \pi)$. We first note that since P is a bounded, self-adjoint operator on $L^2(\mathcal{X}, \pi)$ with norm 1, there exists a projection-valued measure Π, supported on the spectrum $\sigma(P) \subset [-1, 1]$ of P. This measure is known as the spectral resolution of P, and it is defined so that

$$P = \int_{-1}^{1} \lambda \, \Pi(d\lambda).$$

For each $f \in L_0^2(\mathcal{X}, \pi)$, we further define a measure Π_f supported on $\sigma(P) \setminus \{1\}$ by $\Pi_f(d\lambda) := \langle f, \Pi(d\lambda) f \rangle_\pi$. Now, observe that

$$\begin{aligned}
\sigma_f^2 &= \pi(f^2) + 2 \sum_{k=1}^{\infty} E_\pi[f(X_0) f(X_k)] \\
&= \langle f, f \rangle_\pi + 2 \sum_{k=1}^{\infty} \left\langle f, P^k f \right\rangle_\pi \\
&= \langle f, f \rangle_\pi + 2 \left\langle f, P(I - P)^{-1} f \right\rangle_\pi \qquad (4.1) \\
&= \int_{-1}^{1} \frac{1 + \lambda}{1 - \lambda} \Pi_f(d\lambda). \qquad (4.2)
\end{aligned}$$

Using the expression in Equation 4.2, we show that the existence of a positive spectral gap γ is sufficient for the central limit theorem to hold.

Corollary 4.1.1 *Let $(X_n)_{n\geq 0}$ be a Markov chain with Markov transition operator P and stationary measure π. Let $f : \mathcal{X} \to \mathbb{R}$ be a function such that $\pi(f) = 0$ and $\pi(f^2) < \infty$.*

If the Markov chain is reversible and P has spectral gap $\gamma > 0$, then $S_n(f)/\sqrt{n}$ converges in distribution to a centered Gaussian random variable $\mathcal{N}(0, \sigma_f^2)$.

Proof Since P has spectral gap, there exists $0 < \rho < 1$ such that for every $\lambda \in \text{supp}\,(\Pi_f)$, $\lambda \leq \rho$. Therefore, σ_f^2, as given by Equation 4.2, is finite since

$$\sigma_f^2 \leq \frac{1+\rho}{1-\rho}\pi(f^2) < \infty.$$

■

4.2 The Markov-Poisson equation

The expression for the diffusivity given in Equation 4.1 also suggests a new approach for computing σ_f^2 by solving the *Markov-Poisson equation*

$$Lg = -f, \tag{4.3}$$

where $L := P - I$ is the *Markov Laplacian*. In the subsections that follow, we attempt to carry out this program by approximating L using an elliptic differential operator $\mathcal{L}$ whose spectral theory is well understood. We will see that the $\mathcal{L}$ we introduce is in fact the Laplacian on the 2-sphere, and our approximate solutions to the Markov-Poisson equation will arise from solutions of the classical *Poisson equation*

$$\mathcal{L}g = -f. \tag{4.4}$$

Before going on, we briefly remark on an observable of particular interest. Consider a macroscopic billiard table consisting of two parallel, horizontal lines which are $2r$ units apart for any $r > 0$. We call this table a *channel* of radius r. The observable of interest

here will be the *distance traveled* by a particle along its horizontal axis. That is, if the particle starts along one boundary line, we consider the observable that gives the distance traveled in the direction parallel to the boundary until the opposite boundary line is reached by the particle. It is easy to see that this observable is given by $f : (-1, 1) \to \mathbb{R}$ where

$$f(x) = 2r \cot(\cos^{-1} x) = 2rx(1 - x^2)^{-1/2}. \tag{4.5}$$

A small calculation shows that f has mean 0, but infinite variance with respect to the stationary measure. Therefore, the limit theorem with $\sqrt{n}$ scaling given in Theorem 4.1.1 does not apply directly here. Instead we consider a modified, cut-off version of the observable to be defined as in Equation 2.1, i.e. for any $c > 0$, let

$$f_c(x) := f(x)\mathbb{1}_{[|f(x)|\leq c]}(x) + c\mathbb{1}_{[|f(x)|>c]}.$$

4.3 Diffusion approximation and diffusivity

Our aim now is to show that it is possible to approximate the solution of the Markov-Poisson equation $Lg = -f$ for a large class of random billiard micro-structures. We consider families of micro-structures indexed by a scalar quantity h that, in a sense to be made precise, characterizes a key geometric feature of the microscopic billiard cell, namely its flatness. For each micro-structure with parameter h, the corresponding Markov operator P_h will define the dynamics of the random billiard Markov chain as discussed previously. The key idea will be that for small values h, the operator P_h will act nearly like the identity operator, due to the flatness of the geometry. In turn, we study the operator Markov-Laplace operator $L_h := P_h - I$ in the limit as $h \to 0$ and see that under

some general assumptions on the microscopic billiard cell, L_h can be approximated by the classical spherical Laplacian, whose spectral theory is well understood. In the rest of the subsection, we make explicit the necessary assumptions on the geometry and give the statement and proof of our operator approximation result. We conclude the section with an example that shows how geometric parameters such as the curvature arise in the approximation.

Throughout the discussion that follows, we restrict our attention to microscopic billiard cells whose boundary is defined by the graph of a periodic function $F : \mathbb{T} \to \mathbb{R}$. Recall that in a scattering event, we are given a particle with initial unit velocity $v = (\bar{v}, v_0) \in \mathbb{H}^2$ which enters the microscopic billiard cell at a random position $r = (\bar{r}, c) \in \mathbb{T} \times \mathbb{R}$ along the reference line $y = c$. From here, the particle undergoes geodesic motion until reaching the boundary surface at a point $(x, F(x))$. The particle interacts with the boundary surface through specular collision until returning to the reference line when it exits the microscopic billiard cell with a return velocity denoted by $V = (\bar{V}, V_0) \in \mathbb{H}^2$. In order to characterize how flat the micro-structure boundary is, we consider the normal vector field $n : \mathbb{T} \to \mathbb{R}^2$ along the graph of F, and let $\bar{n}$ denote its projection onto its first component. Finally, we let

$$h := \int_{\mathbb{T}} \bar{n}^2 \, dx = \int_0^1 \frac{F'(x)^2}{1 + F'(x)^2} \, dx. \tag{4.6}$$

We will see in examples that follow that h captures information about the curvature of the boundary and for small values of h, the boundary will be relatively flat. In turn, the collision events with the boundary will be relatively simple, often resulting in only

a single collision with the microscopic cell and only resulting in a small perturbation of specular reflection.

We now give a precise statement. Let S_h denote the set of pre-collision vectors in $\mathbb{H}^2$ which result in only one microscopic boundary collision before returning to the reference line. Finally, let $\mathcal{L}$ denote the differential operator acting on smooth functions $\phi : (-1, 1) \to \mathbb{R}$ as

$$\mathcal{L}\phi(\bar{v}) = \frac{d}{d\bar{v}} \left(\left(1 - \bar{v}^2\right) \frac{d}{d\bar{v}} \phi(\bar{v}) \right). \tag{4.7}$$

Theorem 4.3.1 *Let $(F_h)_{h>0}$ be a family of piece-wise smooth functions $F_h : \mathbb{T} \to \mathbb{R}$ defining bilaterally symmetric billiard cells, indexed by the flatness parameter h introduced in Equation 2.3. Let $(P_h)_{h>0}$ be the corresponding Markov transition operators. Then for any $\phi \in C^3(\mathcal{X})$,*

$$L_h\phi(\bar{v}) = 2h\mathcal{L}\phi(\bar{v}) + O\left(h^{3/2}\right),$$

holds for each v such that every initial condition with velocity v results in a trajectory that collides only once with the boundary of the cell.

The differential operator $\mathcal{L}$ has a well understood spectral theory, which in turn will be used to understand the Markov operator P_h in the examples and sections that follow. Here we note a few standard facts

Proposition 4.3.1 *Let $\mathcal{L}$* be the Legendre differential operator defined in Equation 4.7. The following properties hold.

1. *The eigenvalue problem $\mathcal{L}\phi = \lambda\phi$ has solutions if and only if λ is of the form $\lambda = -l(l+1)$ for integers $l \geq 0$.*

2. *The solutions of the eigenvalue problem are the polynomials* ϕ_l, $l \geq 0$, *known as the Legendre polynomials. The first few are given by* $\phi_0 = 1, \phi_1(x) = x, \phi_2(x) = (3x^2 - 1)/2$.

3. *The collection* $(\phi_l)_{l\geq 0}$ *of Legendre polynomials form a complete orthogonal basis for* $L^2(-1, 1)$ *and*

$$\langle \phi_n, \phi_m \rangle := \int_{-1}^{1} \phi_n(x)\phi_m(x)\, dx = \frac{2}{2n+1}\delta_{n,m},$$

where $\delta_{n,m}$ *is the Kronecker delta symbol.*

As a preliminary demonstration of the approximation given in Theorem 2.4.1, we show that it can be used to estimate of the spectral gap of P_h for values of h near 0. Note that the largest eigenvalue of P_h is 1, with eigenfunctions given by the constant functions, and so the the spectral gap of P_h is given by $1 - \lambda$ where λ is the second largest eigenvalue of P_h. Using the approximation in Theorem 2.4.1,

$$P_h\phi_l = (1 - 2hl(l + 1))\, \phi_l + O(h^{3/2}),$$

where ϕ_l is the Legendre polynomial associated to eigenvalue $-l(l + 1)$. This suggests that the second largest eigenvalue λ of P_h is given by

$$\lambda \approx 1 - 4h.$$

We give numerical evidence for this approximation in the next subsection.

We are now ready to discuss the diffusivity σ_f^2 introduced at the start of the section. The idea will be to use the diffusion approximation $\mathcal{L}$ of the Markov-Laplacian L in order to give an approximation of the function $g = (I-P)^{-1}f$ that arises in Equation 4.1. Note that g is a solution of the Markov-Poisson equation $Lg = -f$. We first show that a series

solution of the classical Poisson equation can be given explicitly in terms of Legendre polynomials.

Lemma 4.3.1 *For any $f \in L_0^2(-1,1)$, the equation $\mathcal{L}g = -f$ has solution given by*

$$g = \sum_{l=1}^{\infty} a_l \phi_l, \quad a_l = \frac{2l+1}{2l(l+1)} \langle \phi_l, f \rangle .$$

Proof Let $f \in L_0^2(-1,1)$. Since the Legendre functions form a complete orthogonal basis for $L_0^2(\mathcal{X}, \pi)$, $f = \sum_{l=1}^{\infty} b_l \phi_l$, where $b_l = (2l+1) \langle \phi_l, f \rangle_\pi$. Now, let $g = \sum_{l=1}^{\infty} a_l \phi_l$, where $a_l = b_l/(l(l+1))$. Observe that

$$\mathcal{L}g = \sum_{l=1}^{\infty} a_l \mathcal{L}\phi_l = -\sum_{l=1}^{\infty} a_l l(l+1)\phi_l = -f.$$

■

With the lemma in hand, we now give our main approximation result. The idea of the proof will be to contruct a series solution approximation of the Markov-Poisson equation using the series solution of the Poisson equation along with the diffusion approximation of P. We use the estimates in Theorem 2.4.1 to control the error terms in our approximation.

Theorem 4.3.2 *Let $(P_h)_{h>0}$ be a family of random billiard Markov transition operators for a family of microscopic billiard cells satisfying Assumptions 3.1.1 and 3.1.2. For any function $f \in L_0^2(-1,1)$, let $\sigma_{f,h}^2$ denote the diffusivity corresponding to P_h. Then*

$$\sigma_{f,h}^2 = -\langle f, f \rangle + \frac{1}{h} \sum_{l=1}^{\infty} \frac{2l+1}{l(l+1)} \langle \phi_l, f \rangle^2 + O(h^{1/2}). \tag{4.8}$$

Proof Let $h > 0$ and let g_h be the solution of the Poisson equation $\mathcal{L}g = -f/(2h)$. Note that by Lemma 4.3.1, $g_h = \sum_{l=1}^{\infty} a_{l,h} \phi_l$ where

$$a_{l,h} = \frac{2l+1}{2hl(l+1)} \langle \phi_l, f \rangle .$$

By Theorem 2.4.1, $Lg_h = 2h\mathcal{L}g_h + O(h^{1/2}) = -f + O(h^{1/2})$. Note that the error in the above expression is of lower order than that in the theorem because the right hand side in the Poisson equation contains a factor of h^{-1}. Next observe that

$$\begin{aligned}\langle Pf, g_h\rangle &= \langle f, Pg_h\rangle \\ &= \langle f, g_h\rangle + 2h\,\langle f, \mathcal{L}g_h\rangle + O(h^{1/2}) \\ &= \frac{1}{2h}\sum_{l=1}^{\infty}\frac{2l+1}{l(l+1)}\,\langle \phi_l, f\rangle^2 - \langle f, f\rangle + O(h^{1/2}).\end{aligned}$$

Using the expression above, along with the formula for $\sigma^2_{f,h}$ given in Equation 4.1, the result then follows. ■

Thus the dimensionless self-diffusivity coefficient can be written as

$$\eta_f = -1 + \frac{1}{h}\sum_{l=1}^{\infty}\frac{2l+1}{l(l+1)}\,\langle \phi_l, f/\|f\|_\pi\rangle_\pi^2 + O(h^{1/2}) = \frac{C_f - h}{h} + O\left(h^{1/2}\right), \tag{4.9}$$

where C_f is defined by this identity. The flatness parameter h plays a similar role as the accommodation coefficient ϑ in the Maxwell-Smoluchowski model:

$$\eta = \frac{2-\vartheta}{\vartheta}.$$

The accuracy of the estimate from Equation 4.9 was already shown for the bumps family in Figure 2.4. In Chapter 7 we will explore this approximation further for a variety of other billiard cells.

We end with an example of the billiard cell with microgeometry in Figure 4.1 that consists of a mixture of the small bumps geometry together with flat, specularly reflecting lines. In this case, the family is parameterized by the proportion of initial positions α

that result in reflections with the part of the boundary with curvature. The boundary of of this micro-structure is given by the graph of the function F defined by

$$F(x;\alpha) = \begin{cases} \sqrt{\alpha^2/4 - (x-\alpha/2)^2}, & 0 \le x \le \alpha/2, \\ \alpha/2, & \alpha/2 < x \le 1-\alpha/2, \\ \sqrt{\alpha^2/4 - (x-1+\alpha/2)^2}, & 1-\alpha/2 < x \le 1. \end{cases} \tag{4.10}$$

And the flatness parameter is given by $h = \alpha/3$. Thus, by virtue of Equation 4.9 we expect a good approximation of the dimensionless coefficient of self-diffusion η_f with the expression

$$\eta_f \approx \frac{C_f - h}{h} = \frac{3C_f - \alpha}{\alpha}.$$

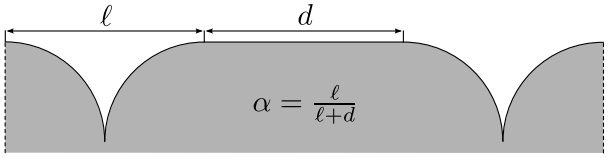

Figure 4.1. Adding a flat segment to a given micro-structure, as indicated in this diagram, gives the transition operator $P_\alpha = \alpha P_1 + (1-\alpha)I$, where P_1 is the operator associated to the original micro-structure.

However, in this example we can derive another expression for η_f in the following way. Consider the transition operator

$$P_\alpha = \alpha P_1 + (1-\alpha)I,$$

where P_1 is the operator associated to an arbitrary micro-structure. Then P_α is associated to the micro-structure for which a segment of horizontal line of length d is added to the billiard cell of the first micro-structure. The parameter α is then the probability that an incoming particle will not collide with the flat segment. It is easy to see the effect

of the additional parameter α. Note that $P_\alpha - I = \alpha(P_1 - I)$. An elementary algebraic manipulation starting from the expression

$$\sigma^2_{f,\alpha} = \langle f, f\rangle + 2\left\langle P_\alpha f, (I - P_\alpha)^{-1} f\right\rangle,$$

gives

$$\eta_{f,\alpha} = \eta_{f,1} + \frac{2(1-\alpha)}{\alpha}\frac{\langle f, (I - P_1)^{-1} f\rangle_\pi}{\|f\|_\pi},$$

where f is arbitrary.

If we decompose the transition operator P for the micro-structure in Figure 4.1 as in the discussion above we can see P_1 is the transition operator for the small bumps micro-structure. As it is to be expected, $\eta_{f,\alpha}$ approaches infinity as the probability of specular reflection increases to 1.

5. Comparison of Variance Estimate Methods

Equation 4.1 provides a method for approximation of the asymptotic variance σ_f^2 by approximating a solution g for the Markov-Poisson equation. Indeed, if g is an approximate solution then

$$\sigma_f^2 \approx \langle f, f \rangle_\pi + 2 \langle f, Pg \rangle_\pi .$$

In the previous chapter we discussed one such method of estimating a solution g. In this chapter we discuss all the methods we've analyzed on this front. Note that an approximation for the asymptotic variance can then be used to approximate the dimensionless diffusion coefficient η by means of Equation 2.2.

1. **Using the differential operator $\mathcal{L}$.** Theorem 4.3.1 and Lemma 4.3.1 provide a solution via an infinite series of Legendre polynomials for a wide class of billiard cells. Truncating this series's first n terms gives us a numerically computational expression; we'll call this approximate solution $g_{\text{Lser},n}$ and the variance estimate using $g_{\text{Lser},n}$ will be denoted by $\sigma^2_{\text{Lser},n}$.

2. **The Galerkin Method**. The discrete Galerkin method uses a finite dimensional approximation of $L^2(\mathcal{X}, \pi)$ in order to obtain a solution to the Poisson equation. Since the orthogonal basis of Legendre polynomials is directly related to P as we discussed previously, sub-spaces of $L^2(X, \pi)$ spanned by finitely many such polynomials give natural finite dimensional sub-spaces to use in the Galerkin method.

The discrete Galerkin method will give us a solution $g_{\mathrm{GM},n}$ that is a linear combination of the first n Legendre polynomials. The variance estimate using $g_{\mathrm{GM},n}$ will be denoted by $\sigma^2_{\mathrm{GM},n}$.

3. **Inverting $I - P$.** Restricting P to $L^2_0(\mathcal{X}, \pi)$ gives us $\|P\|_{\mathrm{op}} < 1$ and so $(I - P)^{-1}$ is given by the usual power series formula. This yields an approximate solution via truncation of the series. The solution from this method will be denoted by $g_{\mathrm{Pser},n}$, with n specifying the truncation. We can also solve the linear system $Lg = -f$ using finite rank approximation of L. This is done via the bi-conjugate gradient stabilized method (BICGSTAB) and denote the solution from this method as g_{BiC}.

A comparison of all the methods we have for estimating the variances is show in Figure 2.6. For small K all of the estimates are comparable, but deviations occur for larger K, in particular for $\sigma^2_{\mathrm{Lser},n}$. A description for discrepancy is given in Section 5.4.

5.1 Legendre series

Our first approximate solution comes from Lemma 4.3.1. Truncating the expression for g gives us a numerical estimate which we will denote by $g_{\mathrm{Lser},n}$.

$$g_{\mathrm{Lser},n} = \sum_{l=1}^{n} a_l \phi_l, \quad a_l = \frac{2l+1}{2l(l+1)} \langle \phi_l, f \rangle . \tag{5.1}$$

The estimate of the asymptotic variance using this approximate solution will be denoted by

$$\sigma^2_{\mathrm{Lser},n} := \langle f, f \rangle_\pi + 2\langle f, P g_{\mathrm{Lser},n} \rangle_\pi.$$

We expect $\sigma^2_{\text{Lser},n}$ to be an accurate estimate when h is small since it is a truncation of the series expansion from Theorem 4.3.2; for large h we expect an error of order $h^{1/2}$.

5.2 The discrete Galerkin method

The *Galerkin method* is a well-known tool for obtaining approximate solutions of equations involving continuous operators, such as in differential operators or, as is the case here, integral operators. The *discrete Galerkin method* specifically refers to the case when numerical integration is used in the derivation of approximate solution. The procedure described below is the method presented in [21].

Let $R_n = \text{span}(\phi_1, \ldots, \phi_n)$, so that $\{R_n : n \geq 1\}$ is a sequence of finite dimensional sub-spaces approximating $L_0^2(\mathcal{X}, \pi)$. And let $T_n : L_0^2(\mathcal{X}, \pi) \to R_n$ denote the orthogonal projection onto R_n.

The Galerkin method for the Poisson equation relative to R_n solves the finite dimensional problem

$$(I - T_n P)g_n = T_n f,$$

for g_n in $L_0^2(\mathcal{X}, \pi)$. Or equivalently, we find g_n in R_n such that

$$\langle (I - P)g_n, \psi \rangle = \langle f, \psi \rangle, \qquad \forall \psi \in R_n. \tag{5.2}$$

It's this latter formulation of the problem we will work with since this can interpreted as follows. By definition of R_n there exists some α_j, $j = 1, \ldots, n$ such that $g_n = \sum_{j=1}^n \alpha_j \phi_j$. Then Equation 5.2 is equivalent to solving for the coefficients α_j in the linear system

$$\sum_{j=1}^{n} \alpha_j \left\{ \langle \phi_j, \phi_i \rangle - \langle P\phi_j, \phi_i \rangle \right\} = \langle f, \phi_i \rangle, \qquad i = 1, \ldots, n. \tag{5.3}$$

Let $G := (\langle \phi_j, \phi_i \rangle - \langle P\phi_j, \phi_i \rangle)_{i,j=1}^n$, and $x := (\alpha_1, \ldots, \alpha_n)^T$, and $y := (\langle f, \phi_1 \rangle, \ldots, \langle f, \phi_n \rangle)^T$ so that the linear system is equivalent to solving $Gx = y$. Let $g_{\mathrm{GM},n}$ denote the solution via the Galerkin method, which will have the form

$$g_{\mathrm{GM},n} = \sum_{k=1}^{n} \alpha_k \phi_k, \tag{5.4}$$

where the α_k are from the vector x defined above. The estimate of the asymptotic variance using $g_{\mathrm{GM},n}$ will be denoted by

$$\sigma^2_{\mathrm{GM},n} := \langle f, f \rangle_\pi + 2\langle f, P g_{\mathrm{GM},n} \rangle_\pi.$$

In fact, we are able to say much more about $g_{\mathrm{GM},n}$. Not only does $g_{\mathrm{GM},n} \to g$ as $n \to \infty$ in $L_0^2(\mathcal{X}, \pi)$, but the rate of convergence is given in [21] as

$$\|g - g_{\mathrm{GM},n}\| \leq \|(I - T_n P)^{-1}\| \|g - T_n g\|. \tag{5.5}$$

This allows us to make the following claim.

Theorem 5.2.1 *Let $f \in L_0^2(\mathcal{X}, \pi)$, where $\mathcal{X} = (-1, 1)$, be such that the first derivative f' is absolutely continuous and the second derivative f'' is of bounded variation. And let P be a transition operator that satisfies the conditions of Corollary 4.1.1 so that σ_f^2 can be defined by the equation*

$$\sigma_f^2 = \langle f, f \rangle_\pi + 2 \left\langle f, P(I - P)^{-1} f \right\rangle_\pi.$$

Then

$$\lim_{n \to \infty} \sigma^2_{\mathrm{GM},n} = \sigma_f^2.$$

Moreover, we have the following rate of convergence:

$$\left| \sigma_f^2 - \sigma^2_{\mathrm{GM},n} \right| \leq \frac{C}{4n - 6},$$

where C is a constant depending on f and P but independent of n.

Remark 5.2.1 *Theorem 5.2.1 can be stated more generally and requiring higher derivatives of f as in Theorem A.3.1 used in the proof. However we've only required conditions on f' and f'' since these are the minimum necessary for the truncated observable f_c to have a definite convergence rate. This also makes it possible for the convergence rate to be written as an explicit function.*

The convergence rate given in Theorem 5.2.1 can be visualized with the following numerical experiment. The asymptotic variance σ_f^2 is unknown, but the sequence $\{\sigma^2_{\mathrm{GM},n}\}_{n=1}^N$ with stabilize when N is large. When $|\sigma^2_{\mathrm{GM},N} - \sigma^2_{\mathrm{GM},N-1}| < 10^{-4}$ we can use $\sigma^2_{\mathrm{GM},N}$ as a proxy for σ_f^2. In our experiment using the transition operator P associated with the bumps family billiard cell with micro-structure parameter with $K = 2$, this tolerance level is achieved with $N = 50$. The results are pictured in the Figure 2.5

5.3 Inverting a finite rank estimate of $(I - P)$

5.3.1 Geometric series

Recall that we have restricted P to $L^2_0(\mathcal{X}, \pi)$, the space of functions in $L^2(\mathcal{X}, \pi)$ with mean zero with respect to π. This restriction gives us $\|P\|_{\mathrm{op}} < 1$ since $\lambda = 1$ is no longer an eigenvalue of P. Thus, we can now compute the inverse of $(I - P)$ with the familiar geometric series.

$$(I - P)^{-1} = \sum_{i=0}^{\infty} P^i. \tag{5.6}$$

With this inverse in hand, we can easily solve the Markov-Poisson equation with $g = \sum_{i=0}^{\infty} P^i f$. Since we do not have a tractable form of P necessary to make use of Equation 5.6 to find an expression for $(I - P)^{-1}$ we can instead get an approximate inverse by truncating the infinite series. This is how we construct the approximate solution $g_{\mathrm{Pser},n}$ which is defined by

$$g_{\mathrm{Pser},n} = \sum_{i=0}^{n} P^i f. \tag{5.7}$$

The variance estimate using this approximate solution will be denoted by

$$\sigma^2_{\mathrm{Pser},n} := \langle f, f\rangle_\pi + 2\langle f, P g_{\mathrm{Pser},n}\rangle_\pi.$$

Although $g_{\mathrm{Pser},n}$ grants us a simple expression for the solution to the Markov-Poisson equation it is computationally expensive in practice. Indeed, since π is the limiting distribution for P, for large n we have $P^n f \approx \pi(f) = 0$. However, the rate at which P approaches its stationary distribution varies greatly. In the case of the bumps billiard cell this can be quantified in terms of the spectral gap and the scale-free curvature parameter K. By Theorem 3.2.1 the convergence rate is controlled by $C(1-\gamma)^n$, for some constant C, where γ is the spectral gap. Thus, to achieve convergence up to a precision $p > 0$ we would need to take

$$n \approx \frac{\log(p/C)}{\log(1-\gamma)}. \tag{5.8}$$

Our numerical estimates (see Figure 2.4) suggest that for the small bumps family the spectral gap decays as $K^2/3$ whenever K is small. Hence, n from Equation 5.8 would be large for small curvature values of K. As an example, for a precision $p = 0.001$ and scale-free curvature $K = 0.1$ we need $n \approx 2,000$. And for our smallest computed curvature $K = 0.03$ we would need $n \approx 23,000$. Storing such a large number of matrices, and much

less computing so many matrix powers, is beyond the computational capacity available to us. Notice that for the example in Figure 2.6 we computed 10^4 terms of the series and its performance is just comparable to the rest. Nevertheless, $\sigma^2_{\mathrm{Pser},n}$ has a theoretical convergence rate, but for the reasons just discussed, it is not as efficient as the rate for the Galerkin method estimate given in Theorem 5.2.1.

Proposition 5.3.1 *For f in $L^2_0(\mathcal{X},\pi)$*

$$\lim_{n\to\infty} \sigma^2_{\mathrm{Pser},n} = \sigma^2_f,$$

and we have

$$|\sigma^2_{\mathrm{Pser},n} - \sigma^2_f| \leq C_n \|f\|^2_{L^2(\mathcal{X},\pi)},$$

where

$$C_n = \sum_{i=n+1}^{\infty} \|P\|^i_{\mathrm{op}}.$$

5.3.2 Bi-conjugate gradient stabilized method

With a finite rank approximation of P we can solve the Markov-Poisson equation simply by matrix inversion. Let P_m denote the matrix approximation of P given to use by discretizing the state space $\mathcal{X}$ into m bins. This is the approach described in detail in Chapter 6. With f_m and g_m the corresponding vector representations of f and g, respectively, the Markov-Poisson equation becomes

$$(P_m - I_m)g_m = -f_m, \tag{5.9}$$

with I_m denoting the $m \times m$ identity matrix. The previous two methods $g_{\mathrm{GM},n}$ and $g_{\mathrm{Pser},n}$ both restricted P to $L^2_0(\mathcal{X},\pi)$ so that we would have $\|P\|_{\mathrm{op}} < 1$. However, our finite

rank estimation method for computing P does follow this technique. As a result, the matrix P_m will have one as an eigenvalue and thus $P_m - I_m$ will not be invertible. In any case it is still possible to choose a solution for the linear system in Equation 5.9. We explored techniques such as least squares methods via the Moore-Penrose inverse and singular value decomposition approximations, but we found the most consistent results with the bi-conjugate gradient stabilized method (BICGSTAB).

BICGSTAB is a combination of the method of successive over-relaxation and the conjugate gradient squared method. It's an iterative method that seeks to minimize the residual error of guesses along two directional vectors - which is what differentiates it from other conjugate gradient method, see [22] for more details. We use Scipy's [23] BICGSTAB implementation of this algorithm. The pseudo-code for this implementation is provided at the end of this chapter.

We let g_{BiC} denote the approximate solution of the Poisson equation from this method. In our computations we use $m = 500$; see Chapter 6 for a detailed description on how P_m is constructed. The resulting estimate of the asymptotic variance by using solution is given by

$$\sigma^2_{\text{BiC}} := \langle f, f \rangle_\pi + 2\langle f, P g_{\text{BiC}} \rangle_\pi.$$

The BICGSTAB method is the most efficient method in terms of computation time for estimating the asymptotic variance, with convergence after less than ten iterations. The performance of most iterative methods depends on the condition number of the

coefficient matrix. For a matrix A let s_1 and s_2 denote the largest and smallest nonzero singular values, respectively; the condition number $\text{cond}(A)$ is defined as

$$\text{cond}(A) = \frac{s_1}{s_2}. \tag{5.10}$$

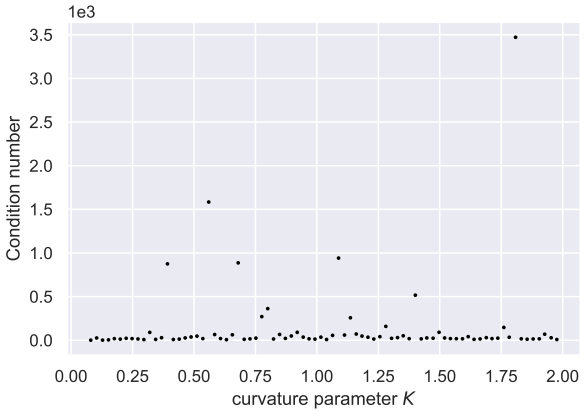

Figure 5.1. The condition numbers of the finite rank matrices for the small bumps family as the curvature parameter K varies.

For BICGSTAB a matrix A is ill-conditioned when $\text{cond}(A) > 10^4$ and will have issues converging to a solution. The singular values for the finite rank approximations of P for the case of the small bumps micro-structure are shown in Figure 5.1. We can see they are well under the threshold and so the problem is well-conditioned in all of our computations.

5.4 Comparing $g_{\mathrm{GM},n}$ and $g_{\mathrm{Lser},n}$

We now take a second look at Figure 2.6 in order to analyze the deviations for large K. Recall that

$$\sigma^2_{\mathrm{GM},n} = \langle f, f\rangle + 2\langle f, Pg_{\mathrm{GM},n}\rangle,$$

$$\sigma^2_{\mathrm{Lser},n} = \langle f, f\rangle + 2\langle f, Pg_{\mathrm{Lser},n}\rangle.$$

So we see that any difference in the variance estimate comes from differences in $g_{\mathrm{Lser},n}$ and $g_{\mathrm{GM},n}$. These two solutions are easily comparable because they are both given as sums of Legendre polynomials given by

$$g_{\mathrm{GM},n}(x) = \sum_{i=1}^{n} \alpha_i \phi_i(x),$$

where the α_i are determined by the Galerkin method. And

$$g_{\mathrm{Lser},n} = \sum_{l=1}^{n} a_l \phi_l, \quad a_l = \frac{2l+1}{2l(l+1)} \langle \phi_l, f\rangle .$$

One thing to note is that $g_{\mathrm{Lser},n}$ has an error term with order K for the case of the small bumps micro-structure. Thus, we only expect a good approximation for small K. Moreover, the observable f defined in Equation 4.5 is an odd function so that $\phi_l(x)f(x)$ remains an odd function for even l; whence the inner product $\langle \phi_l, f\rangle = 0$ for even l. This is also the reason for the "stair-step" pattern in Figure 2.5.

For this observable f we can also express the inner product as follows.

Proposition 5.4.1 *For the observable $f(x) = 2rx(1-x^2)^{-1/2}$ we can write the inner product with the Legendre polynomials is terms of the Gamma function.*

$$\langle \phi_\ell, f\rangle_\pi = \frac{\pi^2 r\ell}{2\Gamma\left(\frac{2-\ell}{2}\right)^2 \Gamma\left(\frac{\ell+1}{2}\right)\Gamma\left(\frac{\ell+3}{2}\right)}. \tag{5.11}$$

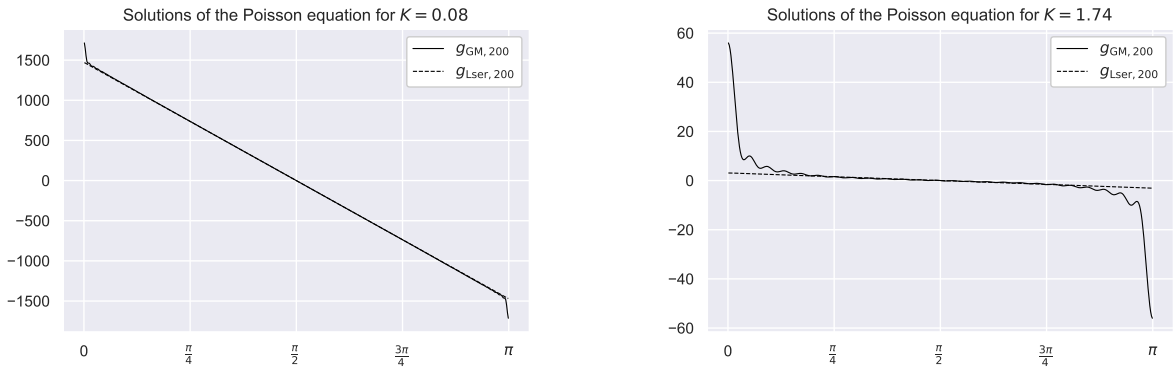

Figure 5.2. The estimated solutions $g_{\mathrm{GM},n}$ and $g_{\mathrm{Lser},n}$ for the Markov-Poisson equation for two values of K for the small bumps micro-structure.

On the other hand, the α_i from $g_{\mathrm{GM},n}$ need not be zero. In fact we observe them to be nonzero in all of our numerical experiments. We find that this is the largest reason for the discrepancies between the two approximate solutions. These differences are highlighted in Figure 5.2 for $n = 200$. This effect causes a larger deviation near to the endpoints. Since f_c is also large near the endpoints, these differences are magnified when computing the asymptotic variance estimates.

Result: A solution to the linear system $A\boldsymbol{x} = \boldsymbol{b}$.

Input: A matrix A and vector $\boldsymbol{b}$, the maximum number of iterations N, a tolerance level $\text{tol} > 0$, and a norm $\|\cdot\|$.

Output: A solution $\boldsymbol{x}_{\text{BiC}}$ to the linear system $A\boldsymbol{x} = \boldsymbol{b}$.

Initialize a (nonzero) guess $\boldsymbol{x}_0$ for the solution of $A\boldsymbol{x} = \boldsymbol{b}$ and set $\boldsymbol{r}_0 = \boldsymbol{b} - A\boldsymbol{x}_0$;

Choose an arbitrary $\boldsymbol{q}_0$ such that $\boldsymbol{q}_0 \cdot \boldsymbol{r}_0 \neq 0$;

Initialize $\boldsymbol{\nu}_0 = \boldsymbol{p}_0 = \boldsymbol{0}$ and $\rho_0 = \alpha = \omega_0 = 1$;

for $i = 1, 2, 3, \ldots N$ **do**

Set $\rho_i = \boldsymbol{q}_0 \cdot \boldsymbol{r}_{i-1}$ and $\beta = \rho_i \alpha / (\rho_{i-1} \omega_{i-1})$;

Update $\boldsymbol{p}_i = \boldsymbol{r}_{i-1} + \beta(\boldsymbol{p}_{i-1} - \omega_{i-1}\boldsymbol{\nu}_{i-1})$;

Update $\boldsymbol{\nu}_i = A\boldsymbol{p}_i$, $\alpha = \rho_i / (\boldsymbol{q}_0 \cdot \boldsymbol{\nu}_i)$, and set $\boldsymbol{h} = \boldsymbol{x}_{i-1} + \alpha \boldsymbol{p}_i$;

if $\|A\boldsymbol{h} - \boldsymbol{b}\| \leq \text{tol}$ **then**

return $\boldsymbol{x}_{\text{BiC}} := \boldsymbol{h}$;

end

Set $\boldsymbol{s} = \boldsymbol{r}_{i-1} - \alpha \boldsymbol{\nu}_i$ and $\boldsymbol{t} = A\boldsymbol{s}$;

Update $\omega_i = (\boldsymbol{t} \cdot \boldsymbol{s}) / (\boldsymbol{t} \cdot \boldsymbol{t})$ and $\boldsymbol{x}_i = \boldsymbol{h} + \omega_i \boldsymbol{s}$;

if $\|A\boldsymbol{x}_i - \boldsymbol{b}\| \leq \text{tol}$ **then**

return $\boldsymbol{x}_{\text{BiC}} := \boldsymbol{x}_i$;

end

Update $\boldsymbol{r}_i = \boldsymbol{s} - \omega_i \boldsymbol{t}$;

end

return $\boldsymbol{x}_{\text{BiC}} := \boldsymbol{x}_N$;

Algorithm 1: Scipy's implementation of BICGSTAB as it is described in the source code, see [24].

6. A finite rank estimation of P

For all of our numerical simulations we work with a finite rank approximation of P. Our approximation is motivated by Equation 3.1 and the discussion at the beginning of Chapter 2.2. In this chapter we describe this approximation in more detail. We also give evidence for the numerical consistency and stability of our methods.

6.1 Collisions in the billiard cell

The first step is simulating collisions in a billiard cell as described in Section 2.1. For simplicity we only consider micro-structures composed of line segments and portions of circles. Despite this limitation, the scope is quite large. In addition we can specify a boundary segment with one (or two) of labels below for further flexibility.

1. **boundary**: The segment is part of the micro-structure and collision is performed in the usual way.

2. **reentry**: These segments are necessary for achieving periodicity. Upon collision the particle "reenters" the billiard cell from the opposite side and continues with unchanged velocity.

3. **exit**: The segment is an exit boundary. The exit angle is recorded and the particle exits the cell, i.e. the simulation of collisions ends.

4. **entrance**: The segment from which a particle can enter. Typically this will be the same as an exit segment, but not necessarily.

Once the boundary is specified we can simulate specular reflections in the billiard cell using elementary vector calculus for any initial condition of the phase space $\mathcal{V} = \mathbb{T} \times \mathcal{X}$, i.e. for any particle entering into the billiard cell at a point $x \in \mathbb{T}$ from the entrance line with velocity $\theta \in \mathcal{X}$.

6.2 The finite rank approximation of P

A separate library of functions simulate the necessary collisions in the billiard cell in order to estimate the transition operator P. The complete procedure for obtaining a finite rank approximation of P is outlined below.

1. Specify a billiard cell M with phase space $\mathcal{V} = \mathbb{T} \times \mathcal{X}$.

2. Partition $\mathbb{T}$ and $\mathcal{X}$ into N and M evenly spaced sub-intervals, respectively. For each sub-interval in the partitions of $\mathbb{T}$ and $\mathcal{X}$ choose a representative, e.g. the midpoint, to construct the sequences $\{r_k\}_{k=1}^{N}$ and $\{\theta_k\}_{k=1}^{M}$, respectively.

3. For each pair (θ, r) in the set $\{(\theta_i, r_j) \ : \ 1 \leq i \leq M, 1 \leq j \leq N\}$ we record the outgoing angle of a particle exiting the billiard cell M after having entered with velocity θ and at r of the entry segment. This is a total of MN simulations.

4. The finite rank approximation of P is then obtained as the $M \times M$ matrix where the ij-th entry of is the proportion of particles that entered the billiard cell with

velocity θ_i and left at an velocity within the range of the sub-interval for which θ_{j+1} represents.

We'll denote by P_M the finite rank approximation of P generated from this method. Note that the parameter M will determine the dimension of the matrix. In our numerical simulations we use $N = 10^4$ and $M = 500$ so that P_M is a 500×500 matrix.

6.3 Numerical consistency

An analysis of how sensitive our estimate P_M is to the parameters M and N. Our target P is the transition operator associated with the small bumps micro-structure. For each finite rank approximation we compute the asymptotic variance with the BICGSTAB method. The results are summarized in Figure 6.1.

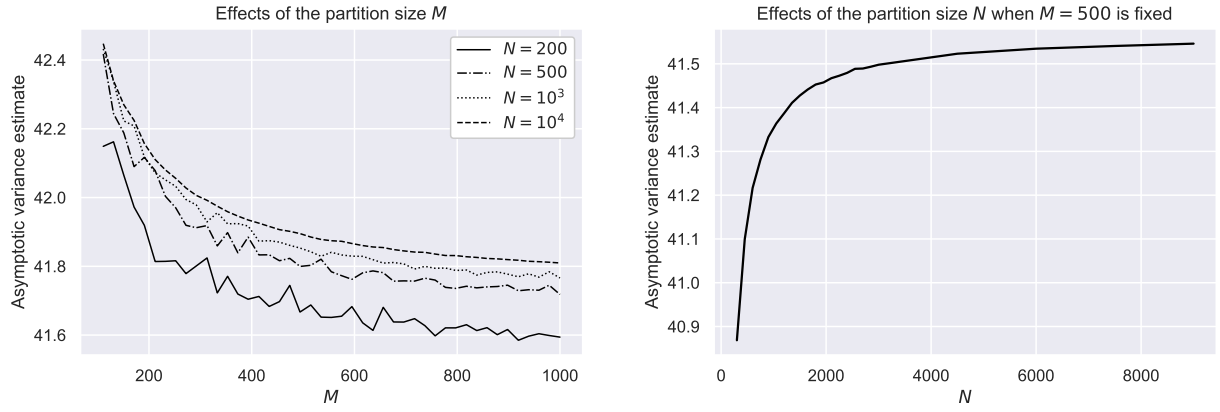

Figure 6.1. Visualizing the effects of the partition of the entry space. In this simulation we took $K = 2$.

The parameter with the strongest effect is the partition size N for $\mathbb{T}$. Small values of N produce inconsistent results as M varies. When it is sufficiently large the behavior is much more stable. The reasoning for our choice of $M = 500$ and $N = 10^4$ can be

seen on the left of Figure 6.1. For $N = 10^4$ variance estimate is sufficiently smooth as M increases; and we see the sharpest changes in the variance estimate as M increases to 300 and then levels off. The range most adhering to the heuristic of "maximum gain" for parameter selection is around $400 - 600$, and so we arrive at $M = 500$. On the right hand side of Figure 6.1 also see that this choice of parameters is optimal in the sense that good stabilization is reached for the variance estimate.

Another performance measure is how fast P_M approaches the stationary distribution $\pi(d\theta) = \sin(\theta)/2 \; d\theta$. We visualize this convergence by plotting the probability density kernel of P_m against $\pi(d\theta)$. The results are shown in Figure 6.2 for various powers of P_M. As discussed earlier, we expect fast convergence large values of K. And indeed, note how fast the kernel converges to the stationary distribution.

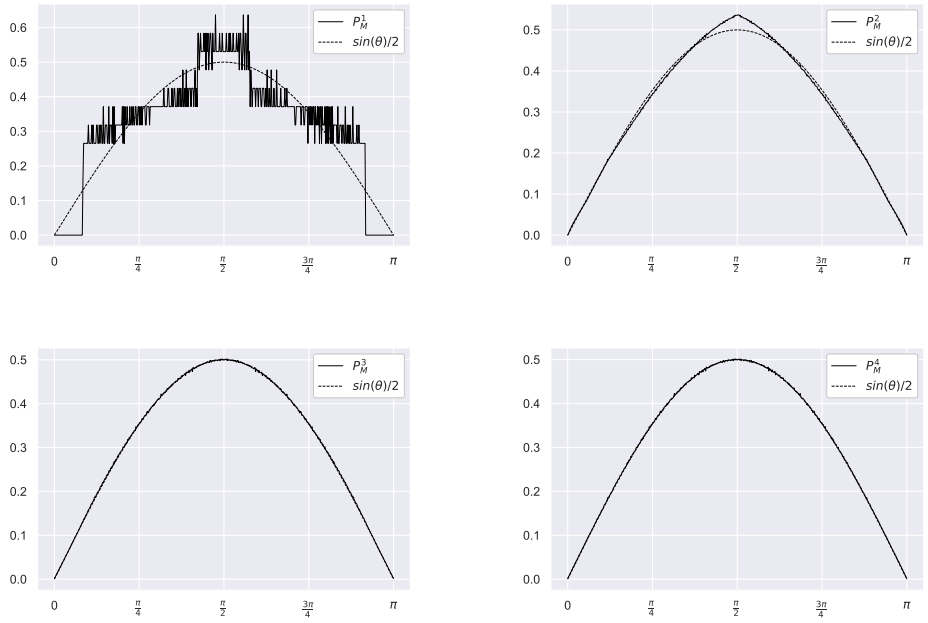

Figure 6.2. The proportion of exit velocities for an entry velocity of $\pi/2$ as given by P_m. The billiard cell is the bumps family with curvature $K = 2$

7. Examples of other billiard cells

In this section we introduce a gallery of different billiard cells and their properties which we've explored with numerical simulations. In these examples we emphasize certain geometric features of the boundary and study how they impact the dimensionless coefficient of self-diffusivity $\eta := \eta_f$.

7.1 The bumps family with a wall

We begin with variations of the bumps family introduced earlier. Because we have a more detailed study of the bumps family, adding variations give insight about the effects of added or removed geometric features. For this first example we add a wall of height a between the bumps with a specified thickness w. The billiard cell has three parameters given by $R \geq 1/2$ for the radius of the semi-circle arcs, $a \geq 0$ for the height of the wall, and $w \geq 0$ for the width of the wall. A visual depiction of this billiard cell is shown in Figure 7.1. Due to the vertical lines of the wall the flatness parameter h for this billiard cell cannot defined since the boundary is be given by a graph of a proper function. This point will be discussed further when we focus on the parameter w in detail in Section 7.1.2

This billiard cell first appeared in [25] where the spectral properties of the transition operators were studied. For example, let $P_{a,w}$ denote the transition operator for the

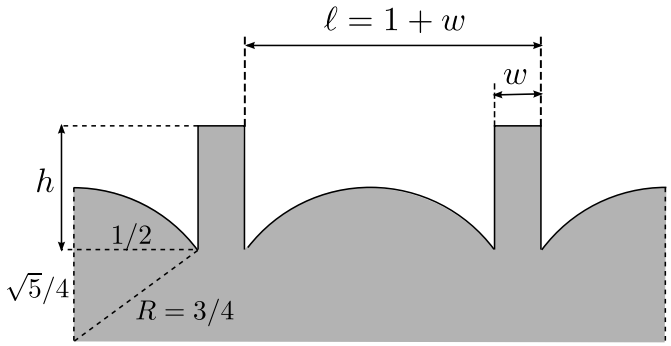

Figure 7.1. The bumps family cell with a wall between the bumps.

bumps with wall billiard cell with wall height a and width w It's shown in [25] that $P_{a,w}$ can be decomposed as

$$P_{a,w} = \frac{2R}{2R+w} P_{a,0} + \frac{w}{2R+w} I.$$

This then leads to the following relationships between the spectral gaps of the operators $P_{h,w}$ and $P_{h,0}$

$$\gamma(P_{a,w}) = \frac{2R}{2R+w} \gamma(P_{a,0}).$$

In the following sections we analyze the effect of a and w on the dimensionless coefficient of self-diffusivity η.

7.1.1 Varying the height parameter

First we'll vary the height parameter of the wall segment and fix the radius of the small bumps and the wall width. A wall in the billiard cell adds a component for specular reflections. For larger a this effect becomes more dominant. In particular, we observe a sharp transition in the spectral gap and η when the wall height is larger than the height of the bump segments.

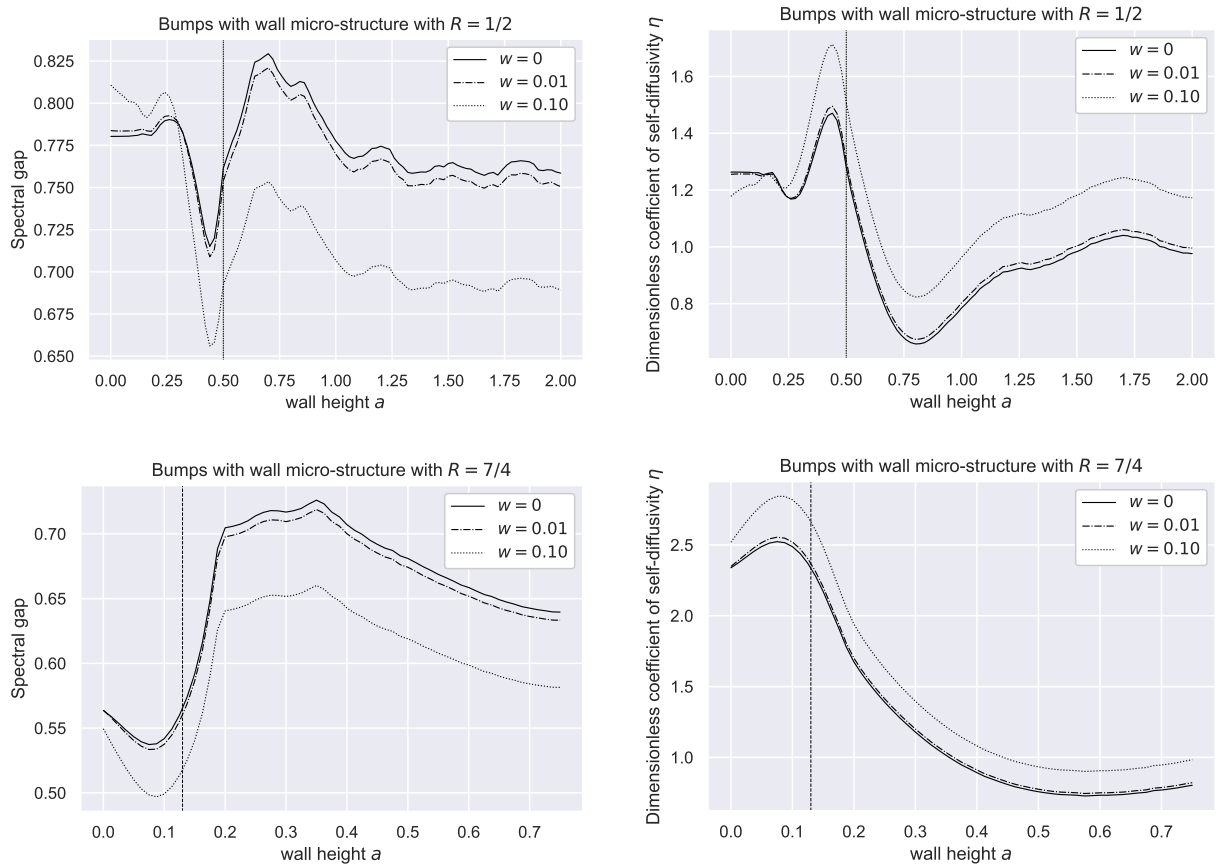

Figure 7.2. The spectral gap and variance for the bumps with wall micro-structure. For the top row we fixed $R = 1/2$ and for the bottom row $R = 7/4$. The vertical dotted line represents the height value at which the height of the wall is level with the height of the bump segment.

Moreover, note the behavior between the cases when $w = 0$ and $w = 0.01$. Since the width is sufficiently small the behavior of the spectral gap and dimensionless coefficient of self-diffusivity are very similar. In comparison, when $w = 0.1$ and the height a is small we see a stronger effect from the flatter geometry.

7.1.2 Varying the width parameter

We now fix the height and instead vary the width of the wall. Having seen the sharp transition when the height of the wall is the same as the curved segment, we set $a = R$ in order to avoid any sharp transitions as we vary the parameter w. As mentioned at the beginning of this section, the boundary of this billiard cell is not given by a proper function; and so Theorem 2.4.2 does not apply. However, we can approximate the wall with smooth functions then we can obtain the parameter h through the following limiting process.

The first step is to describe the wall as a combination of step functions. For example, a wall with base points $(t_1, 0)$ and $(t_2, 0)$ with height a can be described by the *boxcar function* $B_{t_1,t_2}(x)$ given by

$$B_{t_1,t_2}(x) := aH(x - t_1) - aH(x - t_2), \tag{7.1}$$

where H is the Heaviside step function given by $H(x) = \mathbb{1}_{x\geq 0}(x)$. Smooth approximations for the boxcar functions are well known due to their applications in various fields related to life sciences, chemistry, physics, artificial intelligence, etc., see for example [26, 27]. We'll use the following well known approximation using trigonometric functions

$$B_{k,t_1,t_2}(x) := \frac{a}{\pi}(\arctan(k(x - t_1)) - \arctan(k(x - t_2))). \tag{7.2}$$

For these smooth functions B_{k,t_1,t_2} the following point-wise limit holds

$$\lim_{k\to\infty} B_{k,t_1,t_2}(x) = B_{t_1,t_2}(x). \tag{7.3}$$

Thus, the boundary of the bumps with wall billiard cell will be given by the limit $\lim_{k\to\infty} F_k$ where the F_k are defined by

$$F_k(x) = \begin{cases} \sqrt{R^2 - x^2}, & 0 \le x \le w/2, \\ B_{k,t_1,t_2}(x), & w/2 < x \le 1 - w/2, \\ \sqrt{R^2 - (x-1)^2}, & 1 - w/2 < x \le 1. \end{cases} \tag{7.4}$$

For each k the function F_k defines a proper graph for a billiard cell so we can compute h_k i.e.

$$h_= \int_0^1 \frac{F_k'(x)^2}{1 + F_k'(x)^2}\, dx. \tag{7.5}$$

With this informal description of the billiard cell boundary we can consider how the limit of the flatness parameters h_k accurately described the bumps with wall billiard cell. Unfortunately, h cannot be integrated analytically so instead we evaluate it numerically fir $k = 10^3$. Using this estimate we check is approximate the dimensionless coefficient of self-diffusivity η as in Equation 4.9, i.e.

$$\eta \approx \frac{C - h_k}{h_k}.$$

The results are shown in Figure 7.3. The quantity $(C - h_k)/h_k$ displays all the signs of a very coarse estimate - due to the numerical integration errors and the approximation errors of F_k. Overall, however, it follows the same general shape of the η.

7.2 Bumps-and-wall micro-structure

This billiard cell is a variation of the one described in Section 7.1.2, except now the wall is now superimposed on the curved segment, causing the curvature of the billiard cell

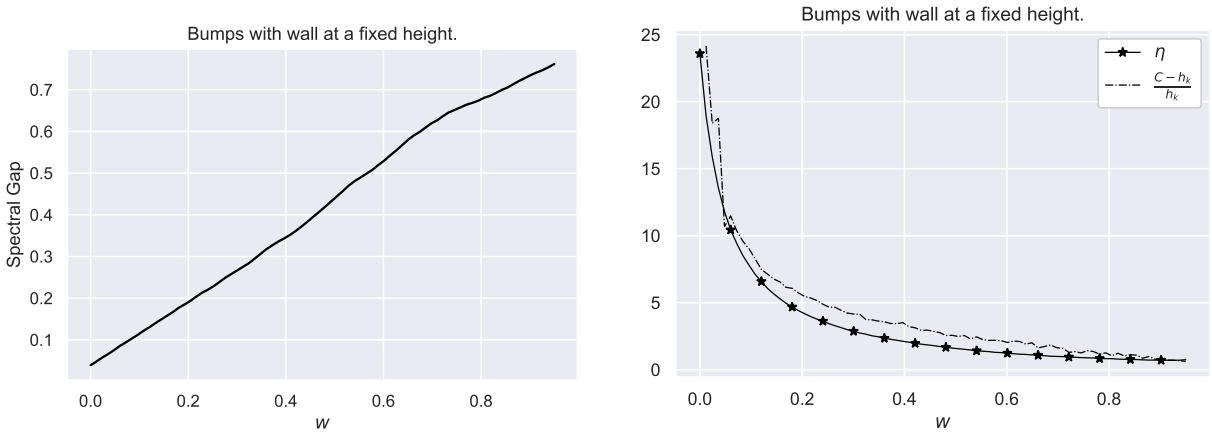

Figure 7.3. The spectral gap and variance for the bumps-and-wall microstructure with fixed radius and height as the width varies. The wall width is specified by $1 - w$. In this example we have $R = a = 1/2$.

to decrease and introduces a flatness component to the boundary. This effect is shown in Figure 7.4.

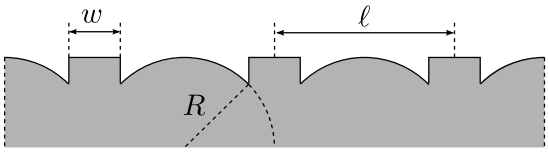

Figure 7.4. A plot of the wall over bumps billiard cell. Note that the wall is superimposed and blocks a portion of the bump segments.

Just as in the previous section, the boundary of this billiard cell cannot be described by the graph of a function due to the wall. Using the boxcar approximation we can approximate the wall in the graph with

$$B_{k,t_1,t_2}(x) := \frac{a}{\pi}(\arctan(k(x-t_1)) - \arctan(k(x-t_2))), \tag{7.6}$$

where $t_1 = w/2$, $t_2 = 1 - w/2$, and $a = R - \sqrt{R^2 - t_1^2}$. And so we can approximate the boundary of the billiard cell with

$$F_k(x) = \begin{cases} \sqrt{R^2 - x^2}, & 0 \le x \le w/2, \\ B_{k,t_1,t_2}(x), & w/2 < x \le 1 - w/2, \\ \sqrt{R^2 - (x-1)^2}, & 1 - w/2 < x \le 1. \end{cases} \tag{7.7}$$

For large k we can estimate the flatness parameter h_k as

$$h_k \approx \int_0^1 \frac{F_k'(x)^2}{1 + F_k'(x)^2}.$$

This computation is done numerically with $k = 10^3$. The resulting estimate of the dimensionless coefficient of self-diffusivity η is shown in Figure 7.2.

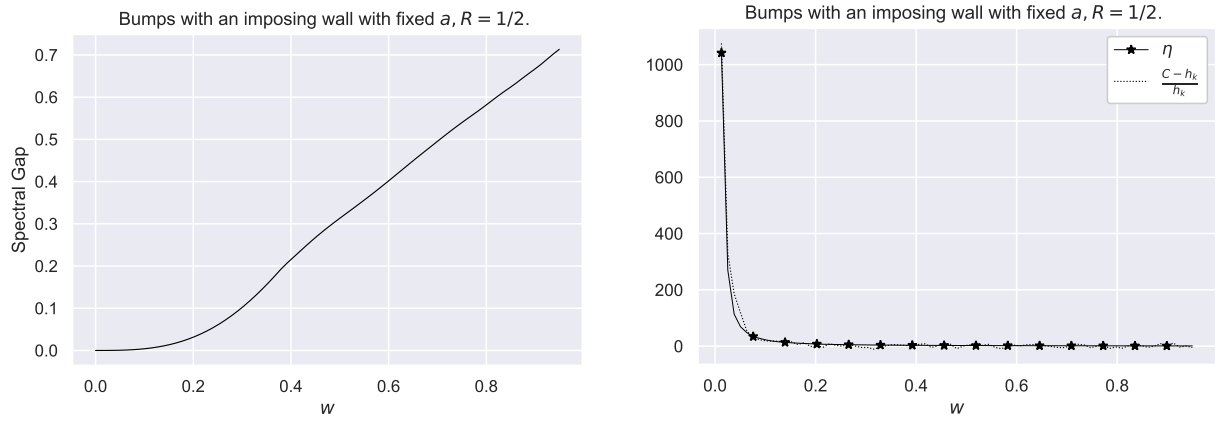

Figure 7.5. The spectral gap and variance for the bumps-and-wall microstructure as the width varies. The width of the flat wall is given by $1 - w$.

7.3 Bumps family with two curvatures

This variation of the bumps family introduces a third bump in the middle on the cell. We refer to this as the *bumps family with two curvatures*. It is parameterized by

$R_1, R_2 > 0$, where R_1 and R_2 specify the radius of each of the two bumps - as shown in Figure 7.6. The boundary is given by the graph of the function F defined by

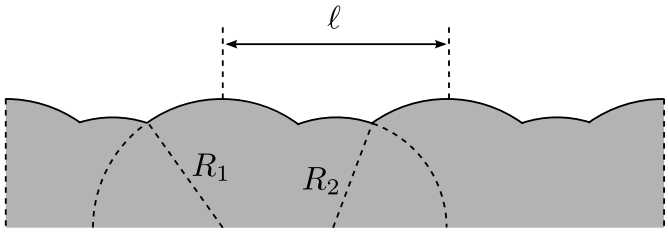

Figure 7.6. A graphical depiction of the bumps family with two curvatures micro-structure.

$$F(x) = \begin{cases} \sqrt{R_1^2 - x^2}, & 0 \le x \le t_1, \\ \sqrt{R_2^2 - (x - 1/2)^2} + y_0, & t_1 < x \le t_2, \\ \sqrt{R_1 - (x-1)^2}, & t_2 < x \le 1. \end{cases} \tag{7.8}$$

where $y_0 = \sqrt{R_1^2 - 1/4}$ and

$$t_2 = \frac{R_2^2 + \sqrt{-4R_2^4R_1^2 + R_2^4 + 16R_2^2R_1^4 - 4R_2^2R_1^2} + 2R_1^2}{4R_1^2}, \qquad t_1 = 1 - t_2.$$

When $R_2 < R_1 - y_0$ we can apply Theorem 2.4.2 to the bumps family with two curvatures billiard cell but when $R_2 > R_1 - y_0$ the bump specified by R_2 becomes the more dominant curved segment since its height is larger than the other and, thus, Theorem 2.4.2 is no longer applicable. In the former case we expect the flatness parameter h to yield a good approximation for the dimensionless coefficient of self-diffusivity η. We can compute the parameter h explicitly, although the resulting expression is rather long. For completeness, it is given in Equation 7.9.

$$
\begin{aligned}
h = \frac{-1}{96R_1^8}\Big(&-8R_1^6 + 48R_1^4R_2^2 - 144R_1^6R_2^2 - 28R_1^2R_2^4 + 84R_1^4R_2^4 + 4R_2^6 \\
&- 12R_1^2R_2^6 16R_1^4\sqrt{R_2^2\left(16R_1^4 - 4R_2^2R_1^2 - 4R_1^2 + R_2^2\right)} \\
&- 16R_1^6\sqrt{R_2^2\left(16R_1^4 - 4R_2^2R_1^2 - 4R_1^2 + R_2^2\right)} \\
&- 16R_1^2R_2^2\sqrt{R_2^2\left(16R_1^4 - 4R_2^2R_1^2 - 4R_1^2 + R_2^2\right)} \\
&+ 4R_1^4R_2^2\sqrt{R_2^2\left(16R_1^4 - 4R_2^2R_1^2 - 4R_1^2 + R_2^2\right)} \\
&+ \left(R_2^2\left(16R_1^4 - 4R_2^2R_1^2 - 4R_1^2 + R_2^2\right)\right)^{3/2} \\
&+3\sqrt{R_2^2\left(16R_1^4 - 4R_2^2R_1^2 - 4R_1^2 + R_2^2\right)}R_2^4\Big).
\end{aligned}
\tag{7.9}
$$

The results of our example are shown in Figure 7.7. The specification is $R_1 = 1.75$ and R_2 is the parameter of interest. Our observations are consistent from with Theorem 2.4.2 in the sense that $(C - h)/h$ is a really good estimate for η when $R_2 < y_0$, but worsens for larger R_2.

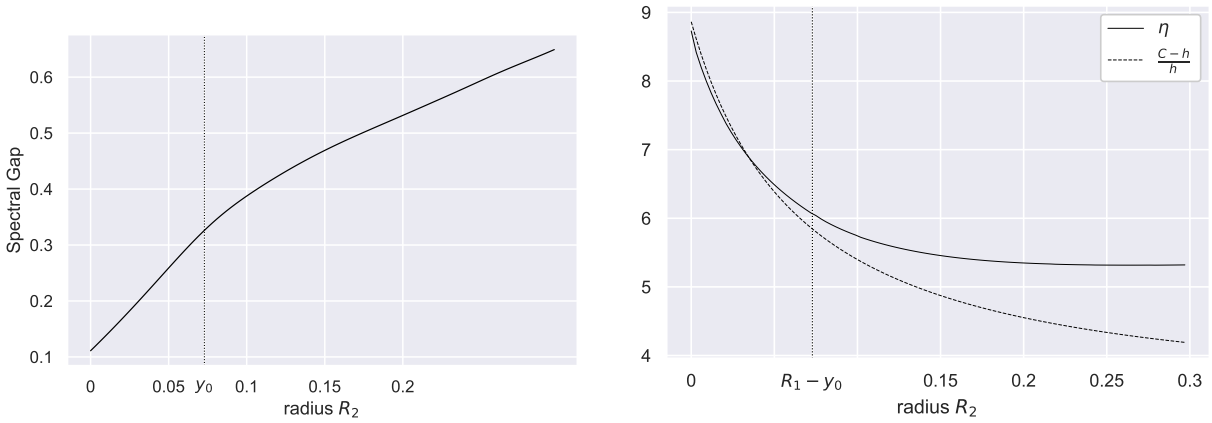

Figure 7.7. The spectral gap (left) and dimensionless coefficient of self-diffusivity (right) for the bumps family with two curvatures microstructure. In this example we fixed $R_1 = 1.75$.

7.4 Circular cavities and flat segments

Our next example is a variation of the billiard cell from depicted in Figure 4.1 which we call the *circular cavities and flat segments* micro-structure. Circular segments of this kinds were previously studied in [28]; for this example we introduce a flat component in between them. A graphical depiction of the billiard cell is given in Figure 7.8.

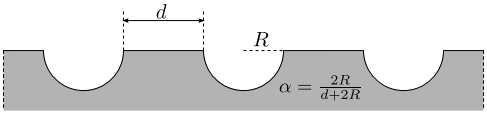

Figure 7.8. The circular cavities and flat segments micro-structure.

This family is specified by a single parameter $0 \leq \alpha \leq 1$. For a given α, the flat component will have length $1 - \alpha$ and the two focusing bumps with have radius $\alpha/2$. Specifically, the boundary of this micro-structure is given by the graph of the function F defined by

$$F(x;\alpha) = \begin{cases} -\sqrt{\alpha^2/4 - x^2}, & 0 \leq x \leq \alpha/2, \\ 0, & \alpha/2 < x \leq 1 - \alpha/2, \\ -\sqrt{\alpha^2/4 - (x-1)^2}, & 1 - \alpha/2 < x \leq 1. \end{cases} \tag{7.10}$$

Notice that Theorem 2.4.2 does not apply to this billiard cell because the curved segments are not concave and are not above a reference line. And thus we do not have an approximation for the dimensionless coefficient of self-diffusion η in terms of the flatness parameter. However, numerical evidence suggests that the dimensionless coefficient of self-diffusivity η is closely approximated by

$$\eta \approx \frac{1-\alpha}{\alpha}.$$

This relationship is depicted in Figure 7.9. Notice how the spectral gap is linear as in the bumps with flat component depicted in Figure 4.1, but much smaller due to the dispersing effect of the curved segments.

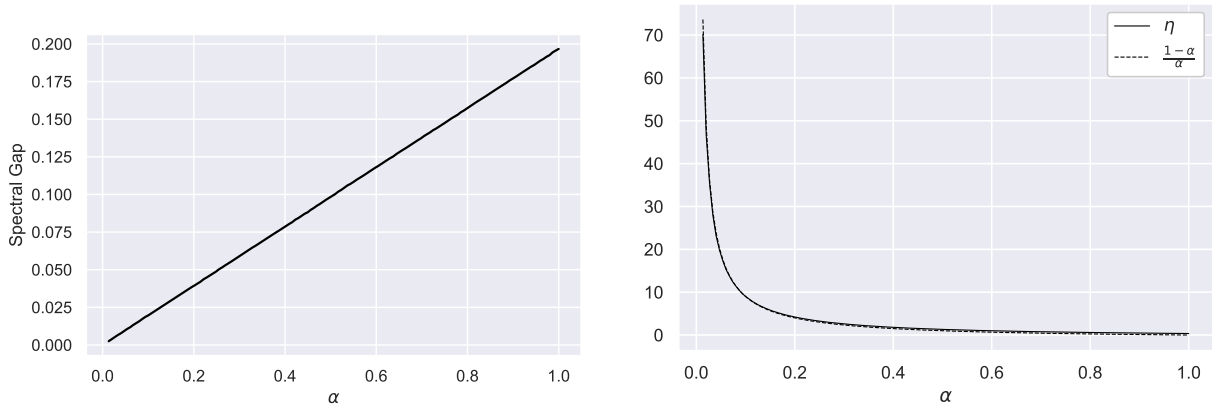

Figure 7.9. The spectral gap (left) and dimensionless coefficient of self-diffusivity (right) for the circular cavities and flat segments micro-structure.

7.5 Two competing curvatures

This family has three parameter: h the height of the two columns, r the radius of the two semi-circles on top of the columns, and R the radius of the large semi-circle segment in the middle. This billiard cell exemplifies two competing curvature constants associated to two arc segments, in the these that one of the curved segments will be more exposed to collisions according to the height parameter h.

We expect that when the high curvature segment is exposed the spectral gap will be large, and a smaller gap when the small curvature segments are exposed. One of the key observations is how sharply the transition occurs.

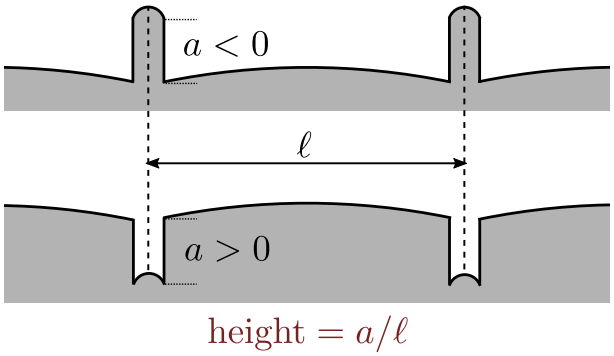

Figure 7.10. Depiction of the multi-parameter family with two competing curvature segments.

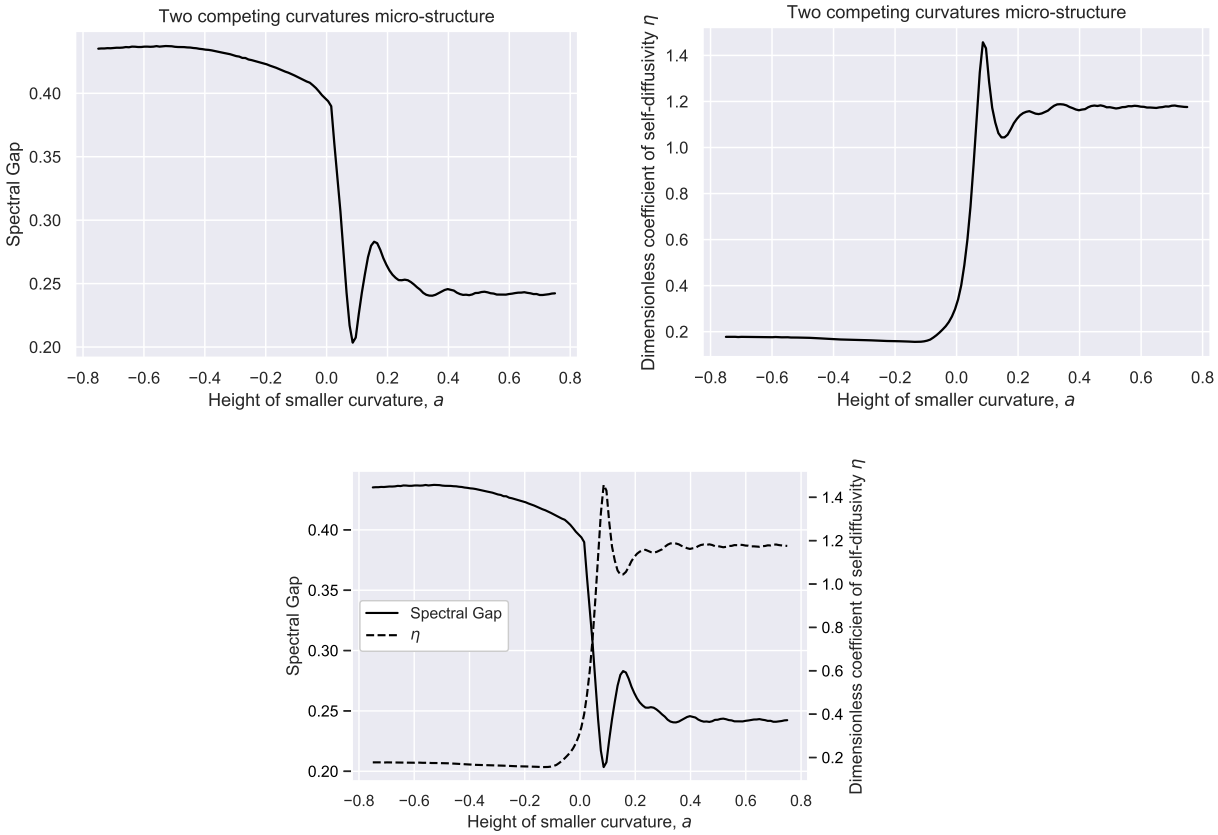

Figure 7.11. The spectral gap (left) and dimensionless coefficient of self-diffusivity (right) for two arcs family. The large radius is set to $R = 2$.

Additionally, notice how mirror-like the spectral gap and the dimensionless coefficient of self-diffusivity behave. In general, we expect faster diffusion when the spectral gap is

small and slower diffusion when the spectral gap is large, but it is surprising that this relationship is so dominant for this micro-structure. Below we plot the spectral gap and dimensionless coefficient of self-diffusivity side-by-side.

APPENDICES

A. Proofs

A.1 Proof of Theorem 2.4.1

Proof When only a single boundary surface collision occurs, the relationship between v and V is straightforward. Indeed, let $n = n(x) = (\bar{n}, n_0)$ denote the vector orthogonal to the boundary surface at the collision point $(x, F(x))$. Then $V = v - 2\langle v, n\rangle n$. Note that by elementary geometry

$$n(x) = \frac{1}{\sqrt{1 + F'(x)^2}} \left(-F'(x), 1\right), \quad \bar{r} = x - \left(F(x) - c\right) \bar{v}/v_0.$$

It now follows that for any smooth function $\phi : (-1, 1) \to \mathbb{R}$

$$\begin{aligned} P\phi(\bar{v}) &= \int_{\mathbb{T}} \phi(\bar{V}(\bar{r}, \bar{v})\, d\bar{r} \\ &= \int_{\mathbb{T}} \phi\left(\bar{v} - 2\langle v, n\rangle \bar{n}\right)\, d\bar{r} \\ &= \int_{\mathbb{T}} \phi(\bar{v} - 2(\alpha + \beta)\bar{n})\left(1 + \alpha/\beta\right)\, dx, \end{aligned}$$

where$\alpha = \bar{n}\bar{v}, \beta = n_0 v_0$. Moreover, for micro-structures satisfying Assumption 3.1.1, the symmetry relations $\bar{n}(-x) = -\bar{n}(x)$ and $n_0(-x) = n_0(x)$ hold and we get

$$P\phi(\bar{v}) = \frac{1}{2}\int_{\mathbb{T}} \left[\phi(\bar{v} - 2(\alpha + \beta)\bar{n})\left(1 + \alpha/\beta\right) + \phi(\bar{v} + 2(-\alpha + \beta)\bar{n})\left(1 - \alpha/\beta\right)\right] dx.$$

From here we use the second order Taylor approximation of ϕ centered about $\bar{v}$. Observe that for $w \in (-1, 1)$

$$\phi(\bar{v} + w) = \phi(\bar{v}) + \phi'(\bar{v})w + \frac{\phi''(\bar{v})}{2}w^2 + R_{\bar{v}}(w),$$

where R is the usual Taylor remain term $R_{\bar{v}}(w) = \phi'''(c)w^3/3!$ for some c in the interval between $\bar{v}$ and w. Using this, together with straightforward algebraic manipulation that we omit for the sake of clarity of exposition, we get that

$$\begin{aligned} P\phi(\bar{v}) &= \phi(\bar{v}) - 4\bar{v}\phi'(\bar{v}) \int_{\mathbb{T}} \bar{n}^2 \, dx + \phi''(\bar{v}) \int_{\mathbb{T}} \bar{n}^2 (6\alpha^2 + 2\beta^2) \, dx + \text{Error}(\bar{v}) \\ &= \phi(\bar{v}) - 4\bar{v}\phi'(\bar{v})h + 2\left(1 - \bar{v}^2\right)\phi''(\bar{v})h + O(h^2) + \text{Error}(\bar{v}) \\ &= \phi(\bar{v}) + 2h\frac{d}{d\bar{v}}\left(\left(1 - \bar{v}^2\right)\phi'(\bar{v})\right) + O(h^2) + \text{Error}(\bar{v}), \end{aligned}$$

where $h = \int_{\mathbb{T}} \bar{n}^2 \, dx$. The error term above arises from the remainder R and is bounded as follows: $|\text{Error}| \leq C_\phi p(\bar{v}) I_3$, where C_ϕ is a constant that depends only on the third derivative of ϕ, $p(\bar{v}, v_0)$ is a polynomial in $\bar{v}, v_0$ of degree at most 3 with coefficients that do not depend on ϕ and $I_3 = \int_{\mathbb{T}} \bar{n}^3$. ■

A.2 Proof of Lemma 3.2.1

We begin by outlining some standard facts in the theory of classical billiards. See [29] for details. Let Γ denote the boundary of the billiard cell Q and note that $\Gamma = \bigcup_i \Gamma_i$ consists of a union of smooth component curves, or walls. We denote by Γ_0 the reference line, which is identified with $\mathbb{T}$. Let $\mathcal{M} = \bigcup_i \mathcal{M}_i$ be the collision space, where each set $\mathcal{M}_i$ consists of pairs (q, v) where $q \in \Gamma_i$ and v points into the interior of Q. Note that the set $N = \bigcup_i N_i$ is the set $\mathcal{M}_0$. The billiard map $\mathcal{F} : \mathcal{M} \to \mathcal{M}$ is the map defined so that $\mathcal{F}(q, v)$ gives the pair (q', v') where q' is the first intersection of the ray $q + tv$, $t > 0$, with ∂Q. The normalized measure $m \otimes \pi \in \mathcal{P}(\mathcal{M})$, where m is the normalized arclength measure on ∂Q, is left invariant by $\mathcal{F}$. Moreover, if we let $T : N \to N$ be the first return map of billiard orbits, the measure $\lambda \otimes \pi$, where λ is the normalized Lebesgue measure on $\mathbb{T}$, is left invariant by T. By Poincaré recurrence, there is a subset $E_0 \subset N$ of full $\lambda \otimes \pi$ measure of orbits that start at and return to Γ_0 in a finite number of steps, and the orbits are non-singular, ie. they do not hit corners of boundary and there are no grazing tangential collisions. As a result, for each $(q, v) \in E_0$, there is an open neighborhood in N whose elements return to N in the same number of steps as (q, v) and the return map on this set is smooth. In the similar fashion, it follows that the map $\Psi_\theta : \mathbb{T} \to \mathcal{X}$ is smooth on an open subset of $\mathbb{T}$ and its restriction to the set W_v^j is likewise a diffeomorphism on an open set which consists of a countable union of open intervals $W_{\theta,i} \subset \mathbb{T}$. It is also the case that for dispersing billiards, eg. those billiards for which ∂Q consists of smooth convex curves with positive curvature, the restriction $\Psi_{\theta,i}$ of Ψ_θ to the set $W_{\theta,i}$ has the

property that $\Psi'_{\theta,i} \neq 0$. Moreover, the summation in Equation 3.3 is well defined; see [29, Lemma 5.56].

We conclude the proof with a verification that the function ω defined in Equation 3.3 is a kernel for P_j. Let $A \subset \mathcal{X}$ be a measurable set and let $A_{\theta,i} = \{x \in W_{\theta,i} : \Psi_{\theta,i}(r) \in A\}$. Then

$$\begin{aligned}
\int_A \omega(\theta,\phi)\,\pi_j(d\phi) &= \frac{1}{\alpha_j(\theta)} \sum_i \int_{A \cap V_{\theta,i}} \left(\frac{1}{2} \left| \Psi'_{\theta,j}\left(\Psi^{-1}_{\theta,j}(\phi)\right) \right| \sin\phi \right)^{-1} \pi(d\phi) \\
&= \frac{1}{\alpha_j(\theta)} \sum_i \int_{\Psi_{\theta,j}(A_{\theta,i})} \left(\left| \Psi'_{\theta,j}\left(\Psi^{-1}_{\theta,j}(\phi)\right) \right| \right)^{-1} d\phi \\
&= \frac{1}{\alpha_j(\theta)} \sum_i \int_{A_{\theta,i}} dr \\
&= P_j \mathbb{1}_A(\theta).
\end{aligned}$$

It follows by a standard argument that P_j has kernel ω for all $f \in L^2(\mathcal{X}, \pi_j)$.

■

A.3 Proof of Theorem 5.2.1

We will make use a recent result by [30] on the decay rates of Legendre series truncation. The result is stated below for completeness.

Theorem A.3.1 (Theorem 2.2 from [30]) *For a function $u : [-1, 1] \to \mathbb{R}$ consider its Legendre series expansion*

$$u(x) = \sum_{i=0}^{\infty} a_i \Phi_i(x), \qquad a_i = \frac{2n+1}{2} \langle u, \Phi_i \rangle.$$

Define the weighted semi-norm

$$\|u\|_{\mathrm{w}} := \int_{-1}^{1} \frac{|u'(x)|}{(1-x^2)^{\frac{1}{4}}}\, dx.$$

Assume that $u, u', \ldots, u^{(m-1)}$ are absolutely continuous and the m-th derivative $u^{(m)}$ is of bounded variation, where derivatives here are defined in the distributional sense. Furthermore, assume that $\|u^{(m)}\|_{\mathrm{w}} < \infty$, then for $n \geq m+1$

$$|a_n| \leq \frac{\|u^{(m)}\|_{\mathrm{w}}}{\sqrt{\pi(2n-2m-1)}} \prod_{k=1}^{m} \left(\frac{2}{2n-2k+1} \right), \tag{A.1}$$

where the product is assumed to be one when $m = 0$.

With this result we are now ready to proof of Theorem 5.2.1.

Proof [Proof of Theorem 5.2.1] First

$$|\sigma_f^2 - \sigma_{\mathrm{GM},n}^2| = |\langle f, f \rangle_\pi - \langle T_n f, T_n f \rangle_\pi \tag{A.2}$$

$$+ 2\langle Pf, g \rangle_\pi - 2\langle T_n P f, g_n \rangle_\pi|. \tag{A.3}$$

For the term in Equation A.2 we see that

$$\begin{aligned}\langle f, f\rangle_\pi - \langle T_n f, T_n f\rangle_\pi &= \|f\|^2 - \|T_n f\|^2 \\ &\leq 2\|f\|(\|f\| - \|T_n f\|) \\ &\leq 2\|f\|\|f - T_n f\|,\end{aligned}$$

which tends to zero as $n \to \infty$ since $f_n = T_n f$ and $\|f\|_{L^2(\mathcal{X},\pi)} < \infty$.

For the term in Equation A.3 we have

$$\begin{aligned}|\langle Pf, g\rangle_\pi - \langle T_n P f, g_n\rangle_\pi| &= |\int [Pf(x)g(x) - T_n P f(x) g_n(x)] d\pi(x)| \\ &= |\int [Pf(x)g(x) - T_n P f(x) g_n(x)] d\pi(x)| \\ &= |\int [(Pf(x)g(x) - Pf(x)g_n(x)) + (Pf(x)g_n(x) - T_n P f(x) g_n(x))] d\pi(x)| \\ &\leq \int |Pf(x)(g(x) - g_n(x))| d\pi(x) + \int |g_n(x)(Pf(x) - T_n P f(x))| d\pi(x) \\ &\leq \|Pf\|\|g - g_n\| + \|g_n\|\|Pf - T_n P f\| \\ &\leq \|Pf\|\|(I - T_n P)^{-1}\|_{\text{op}}\|g - T_n g\| + \|g\|\|Pf - T_n P f\|,\end{aligned}$$

where we used the Holder inequality in the last step.

For $\|Pf - T_n P f\|$ we show that $T_n P = P T_n$. Since P is bounded we can define Pf through the series expansion of $f(x) = \sum_k^\infty b_k \Phi_k(\cos x)$, i.e.

$$Pf(x) = P\left(\sum_{k=1}^\infty a_n \Phi(\cos x)\right) = \sum_{k=1}^\infty a_n P\Phi(\cos x).$$

From this expansion it is clear that

$$T_n P f(x) = \sum_{k=1}^n a_n P\Phi(\cos x) = P T_n f(x).$$

And so we have

$$\|Pf - T_n P f\| = \|Pf - P T_n f\| \leq \|P\|_{\text{op}}\|f - T_n f\|. \tag{A.4}$$

Since $g = (I - P)^{-1} f$ and $(I - P)^{-1}$ is bounded a similar argument also shows

$$\|g - T_n g\| \leq \|(I - P)^{-1}\|_{\text{op}} \|f - T_n f\|. \tag{A.5}$$

It is now evident that the convergence rate will depend on the decay rate of f with it's Legendre series truncation since we've shown

$$|\sigma_f^2 - \sigma_{\text{GM},n}^2| \leq 2\|f - T_n f\|(\|f\| + \|Pf\|)\|(I - P)^{-1}\|_{\text{op}} \|(I - T_n P)^{-1}\|_{\text{op}} + \|g\|)\|P\|_{\text{op}}).$$

The tail of the Legendre series expansion of f is

$$\begin{aligned}
\|f - T_n f\| &= \left\| \sum_{i=n+1}^{\infty} \langle f, \Phi_i \rangle_\pi (2i+1) \Phi(\cos(x)) \right\| \\
&\leq \sum_{i=n+1}^{\infty} |\langle f, \Phi_i \rangle_\pi| (2i+1) \|\Phi(\cos(x))\| \\
&= \sum_{i=n+1}^{\infty} |\langle f, \Phi_i \rangle_\pi| \frac{2i+1}{\sqrt{2i+1}}.
\end{aligned}$$

Note that

$$\langle f, \Phi_i \rangle_\pi \frac{2i+1}{\sqrt{2i+1}} = \frac{2|a_i|}{\sqrt{2i+1}},$$

where a_i is as in Theorem A.3.1 with $u(\cdot) = f(\cos^{-1}(\cdot))$. Applying Theorem A.3.1 with $m = 1$ gives us the bound

$$|a_i| \leq \frac{2\|f'\|_{\text{w}}}{\sqrt{\pi}(2i-1)\sqrt{2i-3}}.$$

Whence the Legendre tail for f can be controlled by

$$\|f - T_n f\| \leq \frac{4 s_n \|f'\|_{\text{w}}}{\sqrt{\pi}}, \tag{A.6}$$

where

$$s_n := \sum_{i=n+1}^{\infty} \frac{1}{(2i-1)\sqrt{2i+1}\sqrt{2i-3}} \tag{A.7}$$

is finite for all $n \geq 0$.

The resulting bound is

$$|\sigma_f^2 - \sigma_{\mathrm{GM},n}^2| \leq \frac{8 s_n \|f'\|_{\mathrm{w}}}{\sqrt{\pi}} \left(\|f\| + \|Pf\| \|(I-P)^{-1}\|_{\mathrm{op}} \|(I - T_n P)^{-1}\|_{\mathrm{op}} + \|g\| \|P\|_{\mathrm{op}} \right).$$

Since $\|T_n P\|_{\mathrm{op}} \leq \|P\|_{\mathrm{op}} < 1$ the inverse $(I - T_n P)^{-1}$ is given by infinite series $(I - T_n P)^{-1} = \sum_{k=0}^{\infty} (T_n P)^k$, which allows us the bound

$$\|(I - T_n P)^{-1}\|_{\mathrm{op}} \leq \frac{1}{1 - \|T_n P\|_{\mathrm{op}}} \leq \frac{1}{1 - \|P\|_{\mathrm{op}}}. \tag{A.8}$$

And so the constant C from the statement of this proposition is now independent of n and is given by

$$C = \frac{8 \|f'\|_{\mathrm{w}}}{\sqrt{\pi}} \left(\|f\| + \frac{\|Pf\| \|(I-P)^{-1}\|_{\mathrm{op}}}{1 - \|P\|_{\mathrm{op}}} + \|g\| \|P\|_{\mathrm{op}} \right). \tag{A.9}$$

Since $g = (I - P)^{-1} f$ we also have the bound $\|g\| \leq \|(I-P)^{-1}\|_{\mathrm{op}} \|f\|$. Moreover, a similar bound holds for the operator norm of $(I - P)^{-1}$ as in Equation A.8.

$$\|(I - P)^{-1}\|_{\mathrm{op}} \leq \frac{1}{1 - \|P\|_{\mathrm{op}}}. \tag{A.10}$$

Thus, we may also have

$$C = \frac{8 \|f'\|_{\mathrm{w}} \|f\|}{\sqrt{\pi}} \left(1 + \frac{\|P\|_{\mathrm{op}}}{(1 - \|P\|_{\mathrm{op}})^2} + \frac{\|P\|_{\mathrm{op}}}{1 - \|P\|_{\mathrm{op}}} \right). \tag{A.11}$$

Lastly, returning to the constant term s_n from Equation A.7, for $n > 2$ we have

$$\begin{aligned} s_n &= \sum_{i=n+1}^{\infty} \frac{1}{(2i-1)\sqrt{2i+1}\sqrt{2i-3}} \\ &< \sum_{i=n+1}^{\infty} \frac{1}{(2i-3)^2} \\ &\leq \int_n^{\infty} \frac{dx}{(2x-3)^2} \\ &= \frac{1}{4n-6}. \end{aligned}$$

■

The first and second derivative of the truncated channel observable f_c is given by

$$f_c'(x) = \frac{2rx}{(1-x^2)^{1/2}} \mathbb{1}_{\{|2rx/(1-x^2)^{1/2}|<c\}}(x)$$
$$f_c''(x) = \frac{6rx}{(1-x^2)^{5/2}} \mathbb{1}_{\{|2rx/\sqrt{1-x^2}|<c\}}(x).$$

So we can compute the semi-norm $\|f'\|_{\mathrm{w}}$ as

$$\begin{aligned}\|f'\|_{\mathrm{w}} &= \int_{-1}^{1} \frac{6r|x|}{(1-x^2)^{11/4}} \mathbb{1}_{\{|2rx/\sqrt{1-x^2}|<c\}}(x)\, dx \\ &= \int_{-a}^{a} \frac{6r|x|}{(1-x^2)^{11/4}}\, dx,\end{aligned}$$

where $a = c/\sqrt{c^2+4r^2}$. Evaluating the integral gives us

$$\|f_c'\|_{\mathrm{w}} = \frac{4}{7}\left[\left(\frac{c^2}{4r^2}+1\right)^{7/4} - 1\right] \tag{A.12}$$

A.4 Proof of Proposition 5.4.1

Lemma A.4.1 *Define*

$$I_n := \int_0^\pi \cos^n(x).$$

When n is odd $I_n = 0$ and when n is even

$$I_n = \frac{1}{2^n}\binom{n}{n/2}\pi = \frac{n!}{2^{n+1}(n/2)!}\pi \tag{A.13}$$

Proof [Proof of Proposition 5.4.1] We'll make use of the following identity of Legendre polynomials.

$$\phi_m(x) = 2^m \sum_{k=0}^{m} x^k \binom{m}{k}\binom{\frac{m+k-1}{2}}{m}, \qquad \forall m \geq 0. \tag{A.14}$$

This allows us to write the inner product as follows.

$$\begin{aligned}
\langle \phi_n, f\rangle_\pi &= r\int_0^\pi \cot(x)\sin(x)\phi_n(\cos(x))\,dx \\
&= r\int_0^\pi \cos(x)\phi_n(\cos(x))\,dx \\
&= 2^n r \sum_{k=0}^{n}\binom{n}{k}\binom{\frac{n+k-1}{2}}{n}\int_0^\pi \cos^{k+1}(x)\,dx.
\end{aligned}$$

By Lemma A.4.1 the integral term can be written in terms of a binomial so that

$$\langle \phi_n, f\rangle_\pi = 2^n r\pi \sum_{k=0}^{n}\binom{n}{k}\binom{\frac{n+k-1}{2}}{n}\left(\frac{1+(-1)^{k+1}}{2^{2k+2}}\right)\binom{k+1}{(k+1)/2}$$

To complete the proof we express the binomials in terms of the Gamma function and we use the multiplicative properties of the Gamma function (see, in particular, identities 99 104, 125 in [31]). ■

REFERENCES

[1] T. Chumley, R. Feres, and H.-K. Zhang. Diffusivity in multiple scattering systems. *Trans. Amer. Math. Soc*, 368(1):109–148, 2016.

[2] G. Arya, H.-C. Chang, and E. J. Maginn. Knudsen diffusivity of a hard sphere in a rough slit pore. *Phys. Rev. Lett*, 91:026102, July 2003.

[3] R. Feres, J. Ng, and H.-K. Zhang. Multiple scattering in random mechanical systems and diffusion approximation. *Comm. Math. Phys*, 323(2):713–745, 2013.

[4] R. Feres. Random walks derived from billiards. In Dynamics, ergodic theory, and geometry*, volume 54 of* Math. Sci. Res. Inst. Publ.*, . Univ. Press, Cambridge*, pages 179–222. 2007.

[5] R. Feres and H.-K. Zhang. Spectral gap for a class of random billiards. *Comm. Math. Phys*, 313(2):479–515, 2012.

[6] C. Kipnis and S. R. S. Varadhan. Central limit theorem for additive functionals of reversible Markov processes and applications to simple exclusions. *Comm. Math. Phys*, 104(1):1–19, 1986.

[7] J. M. Anderson et al. Isothermal mass flow measurements in microfabricated rectangular channels over a very wide knudsen range. *J. Micromech. Microeng*, 24:055013, 2014.

[8] L. Marino. *Experiments on rarefied gas flows through tubes*, 6:109–119, 2009.

[9] P. Perrier, I. A. Graur, T. Ewart, and J. G. Méolans mass flow rate measurements in microtubes: From hydrodynamic to near free molecular regime. *Physics of Fluids*, 23:042004, 2011.

[10] S. Varoutis et al. Computational and experimental study of gas flows through long channels of various cross sections in the whole range of the knudsen number. *J. Vac. Sci. Technol*, 27(1):89–100.

[11] H. Yamaguchi, Y. Matsuda, and T. Niimi. Tangential momentum accommodation coefficient measurements for various materials and gas species. In Journal of Physics: *Conference Series 362 (2012) 012035 1st European Conference on Gas Micro Flows (GasMems*, 2012.

[12] O. Angel, K. Burdzy, and S. Sheffield. Deterministic approximations of random reflectors. *Trans. Amer. Math. Soc*, 365(12):6367–6383, 2013.

[13] C. Barnes, K. Burdzy, and C.-E. Gauthier. Billiards with Markovian reflection laws. *Electron. J. Probab*, 147:32, 2019.

[14] F. Comets, S. Popov, G. M. Schütz, and M. Vachkovskaia. Billiards in a general domain with random reflections. *Arch. Ration. Mech. Anal*, 191(3):497–537, 2009.

[15] S. N. Evans. Stochastic billiards on general tables. *Ann. Appl. Probab*, 11(2):419–437, 2001.

[16] K. Khanin and T. Yarmola. Ergodic properties of random billiards driven by thermostats. *Comm. Math. Phys*, 320(1):121–147, 2013.

[17] S. Cook and R. Feres. Random billiards with wall temperature and associated Markov chains. *Nonlinearity*, 25(9):2503–2541, 2012.

[18] R. Feres and G. Yablonsky. Knudsen's cosine law and random billiards. *Chemical engineering science*, 59(7):1541–1556, 2004.

[19] G. O. Roberts and J. S. Rosenthal. Geometric ergodicity and hybrid Markov chains. *Electron. Comm. Probab*, 2(2):13–25, 1997.

[20] J. Weidmann. *Linear operators in Hilbert spaces*, volume 68. of *Graduate Texts in Mathematics*. Springer-Verlag, New York-Berlin Translated from the German by Joseph Szücs, 1980.

[21] Kendall Atkinson and Alex Bogomolny. The discrete galerkin method for integral equations. *Mathematics of computation*, 48(178):595–616, 1987.

[22] Sou-Cheng T Choi, Christopher C Paige, and Michael A Saunders. Minres-qlp: A krylov subspace method for indefinite or singular symmetric systems. *SIAM Journal on Scientific Computing*, 33(4):1810–1836, 2011.

[23] Pauli Virtanen, Ralf Gommers, Travis E. Oliphant, Matt Haberland, Tyler Reddy, David Cournapeau, Evgeni Burovski, Pearu Peterson, Warren Weckesser, Jonathan

Bright, Stéfan J. van der Walt, Matthew Brett, Joshua Wilson, K. Jarrod Millman, Nikolay Mayorov, Andrew R. J. Nelson, Eric Jones, Robert Kern, Eric Larson, CJ Carey, İlhan Polat, Yu Feng, Eric W. Moore, Jake Vand erPlas, Denis Laxalde, Josef Perktold, Robert Cimrman, Ian Henriksen, E. A. Quintero, Charles R Harris, Anne M. Archibald, Antônio H. Ribeiro, Fabian Pedregosa, Paul van Mulbregt, and SciPy 1. 0 Contributors. SciPy 1.0–Fundamental Algorithms for Scientific Computing in Python. *arXiv e-prints*, page arXiv:1907.10121, Jul 2019.

[24] https://docs.scipy.org/doc/scipy 0.14.0/reference/generated/scipy.sparse.linalg.bicgstab.html. scipy.sparse.linalg.bicgstab. *scipy.sparse.linalg.bicgstab - SciPy v0.14.0 Reference Guide*.

[25] Renato Feres and Hong-Kun Zhang. Spectral gap for a class of random billiards. *Communications in Mathematical Physics*, 313(2):479–515, 2012.

[26] David H Von Seggern. *CRC standard curves and surfaces*. CRC Press, 1992.

[27] Anton Iliev Iliev, Nikolay Kyurkchiev, and Svetoslav Markov. On the approximation of the cut and step functions by logistic and gompertz functions. *Biomath*, 4(2):1510101, 2015.

[28] Timothy Chumley, Renato Feres, and Hong-Kun Zhang. Diffusivity in multiple scattering systems. *Transactions of the American Mathematical Society*, 368(1):109–148, 2016.

[29] Nikolai Chernov and Roberto Markarian. *Chaotic billiards*, volume 127 of *Mathematical Surveys and Monographs*. American Mathematical Society, Providence, RI, 2006.

[30] Haiyong Wang. A new and sharper bound for legendre expansion of differentiable functions. *Applied Mathematics Letters*, 85:95–102, 2018.

[31] Michael Z Spivey. *The art of proving binomial identities*. CRC Press, 2019.